Physiological and head motion signatures in static and time-varying functional connectivity and their subject discriminability

Alba Xifra-Porxas [1,*], Michalis Kassinopoulos [1,*], Georgios D. Mitsis [2]

[1] Graduate Program in Biological and Biomedical Engineering, McGill University, Montréal, Canada

[2] Bioengineering Department, McGill University, Montréal, Canada

* equal contribution

Keywords: physiological processes, head motion, breathing motion, fMRI, functional connectivity, resting-state, fMRI artifacts

Abstract

It is well established that head motion and physiological fluctuations have a pronounced influence on resting-state fMRI activity. Here, we capitalize on a large sample from the Human Connectome Project to provide a comprehensive investigation of the biases in functional connectivity (FC) that arise from head motion, breathing motion, cardiac pulsatility, and systemic low-frequency oscillations (SLFOs) associated with changes in heart rate and breathing patterns. In static FC, artifactual connectivity was found in the sensorimotor network due to head motion, as well as in the visual network due to head motion and SLFOs. Breathing motion was found to increase within-hemisphere connectivity, which was attributed to the phase encoding direction. Recurrent patterns in time-varying FC were found to be partly correlated to head motion and SLFOs. Several preprocessing strategies were examined to assess their capability in mitigating the effects of nuisance processes. Nuisance signatures exhibited above-chance levels of subject discriminability; however, fMRI data corrected for these confounds improved subject identifiability.

1 Introduction

Functional magnetic resonance imaging (fMRI) is based on the blood-oxygenation-level-dependent (BOLD) contrast mechanism (Ogawa *et al.*, 1990), and is widely viewed as the gold standard for studying brain function because of its high spatial resolution and non-invasive nature. The BOLD signal exhibits low frequency (~0.01-0.15 Hz) fluctuations that are synchronized across distant regions of the brain, a phenomenon known as functional connectivity (FC). FC has been observed even in the absence of any explicit stimulus or task, giving rise to the so-called resting-state networks (RSNs) (Biswal *et al.*, 1995; Fox and Raichle, 2007; Smith *et al.*, 2009). Initially, FC was viewed as a stationary phenomenon (static FC) and was commonly measured as the correlation between brain regions over an entire scan. However, several researchers challenged this assumption (Chang and Glover, 2010; Sakoglu *et al.*, 2010), and recent studies have been focusing on FC dynamics, quantified over shorter time scales than the scan duration (time-varying FC) (Hutchison *et al.*, 2013; Lurie *et al.*, 2019).

Although the neurophysiological basis of resting-state FC measured with fMRI is not yet fully understood, many studies have given evidence to support its neuronal origin. For instance, in animal models, a strong association between spontaneous BOLD fluctuations and neural activity, in particular band-limited local field potentials and firing rates, has been reported (Shmuel and Leopold, 2008; Schölvinck *et al.*, 2010; Thompson, Merritt, *et al.*, 2013). Furthermore, a recent study suggested a close correspondence between windowed FC calculated from simultaneously recorded hemodynamic signals and calcium transients (Matsui, Murakami and Ohki, 2018). In human studies, direct measurements of macroscale neural activity demonstrate a spatial correlation structure similar to that of spontaneous BOLD fluctuations (He *et al.*, 2008; Brookes *et al.*, 2011; Hipp *et al.*, 2012; Hacker *et al.*, 2017; Kucyi *et al.*, 2018), even during transient (50-200 ms) events (A. P. Baker *et al.*, 2014; Vidaurre *et al.*, 2018; Hunyadi *et al.*, 2019). Therefore, it is widely assumed that resting-state FC measured in brain hemodynamics reflects spontaneous co-fluctuations of the underlying neuronal networks.

However, it is crucial to bear in mind that BOLD signals rely on changes in local cerebral blood flow (CBF) to infer underlying changes in neuronal activity, and according to a recent study at least 50% of the spontaneous hemodynamic signal is unrelated to ongoing neural activity (Winder *et al.*, 2017). For instance, systemic physiological functions can induce variations in global and local CBF which in turn lead to fluctuations on the BOLD signal. In particular, low frequency variations in breathing activity (Birn *et al.*, 2006, 2008; Power *et al.*, 2017), arterial blood pressure (Whittaker *et al.*, 2019), CO_2 concentration (Wise *et al.*, 2004; Prokopiou *et al.*, 2019), and heart rate (Shmueli *et al.*, 2007; Chang, Cunningham and Glover, 2009) are known to account for considerable variance in the BOLD signal, presumably through changes in CBF. In addition, the BOLD signal intensity is distorted by high-frequency physiological fluctuations, such as cardiovascular pulsation and breathing, through displacement of the brain tissues and perturbations of the B_0 magnetic field (Dagli, Ingeholm and Haxby, 1999; Glover, Li and Ress, 2000). Further, head motion is well-known to have a substantial impact in fMRI through partial

volume, magnetic inhomogeneity and spin-history effects (Friston *et al.*, 1996; Power *et al.*, 2012). These non-neuronal factors may introduce common variance components in signals recorded from different brain regions and subsequently induce spurious correlations between these areas. Therefore, to account for motion-related and physiological confounds, nuisance regressors are typically obtained using model-based and data-driven techniques, and regressed out from the fMRI data before further analysis (Caballero-Gaudes and Reynolds, 2017).

Remarkably, both static and time-varying resting-state FC have shown promise for providing concise descriptions of how the brain changes across the lifespan (Chan *et al.*, 2014; Geerligs *et al.*, 2015; Sala-Llonch, Bartrés-Faz and Junqué, 2015; Ferreira *et al.*, 2016; Battaglia *et al.*, 2017; Xia *et al.*, 2019), and to assay neural differences that accompany disease (Damaraju *et al.*, 2014; J. T. Baker *et al.*, 2014; Hahamy, Behrmann and Malach, 2015; Demirtaş *et al.*, 2016; Du *et al.*, 2016; Chen *et al.*, 2017; Drysdale *et al.*, 2017; Morgan *et al.*, 2017; Xia *et al.*, 2018; Gratton, Koller, *et al.*, 2019; Mash *et al.*, 2019). However, recent studies assessing the performance of a large range of preprocessing strategies found that there is always a trade-off between adequately removing confounds from fMRI data and preserving the signal of interest (Ciric *et al.*, 2017; Parkes *et al.*, 2018; Kassinopoulos and Mitsis, 2019b). Importantly, widely used techniques for preprocessing of fMRI data cannot efficiently remove physiological and motion artifacts. The latter raises a concern as it is still not clear how nuisance fluctuations may impact the outcome of FC studies.

Several studies have examined whether physiological fluctuations across the brain could give rise to structured spatial patterns that resemble common RSNs, based on the evidence that vascular responses following systemic changes are spatially heterogenous (Chang, Cunningham and Glover, 2009; Pinto *et al.*, 2017), or account for the observed time-varying interactions between RSNs. For instance, (Bright and Murphy, 2015) applied independent component analysis (ICA) to the fraction of the fMRI data explained by nuisance regressors related to head motion and physiology and revealed a characteristic network structure similar to the previously reported RSNs. Similarly, (Tong *et al.*, 2013; Tong and Frederick, 2014) found significant contributions of systemic fluctuations on ICA time courses related to visual, sensorimotor and auditory networks. Recently, (Chen, Lewis, *et al.*, 2019) generated BOLD data containing only slow respiratory-related dynamics and showed that respiratory variation can give rise to seeming neurally-related connectivity patterns. Further, recent investigations have shown that physiological confounds can modulate time-varying FC measures (Chang *et al.*, 2013; Nikolaou *et al.*, 2016; Nalci, Rao and Liu, 2019). These results suggest that changes in brain physiology, breathing patterns, heart rhythms and head motion across sessions within-subject or across populations can introduce artifactual inter-individual and group-related differences in FC independent of any underlying differences in neural activity. Therefore, the disentanglement of the neural and physiological correlates of resting-state FC is decisive for increasing its clinical impact.

While the previous findings provide evidence for the dual-nature of RSNs in both static and time-varying scenarios, only specific physiological processes and/or particular brain networks were evaluated in each of the aforementioned

studies. A more holistic assessment of the impact of these non-neural processes on FC measures is needed to better understand whether and how systemic fluctuations and head or breathing motion affect inter-individual and group differences as well as evaluation and comparison of the impact of proposed preprocessing solutions.

The inefficacy of preprocessing pipelines to completely remove physiological fluctuations has also implications for studies investigating properties of FC at the individual level. Recent reports have shown that connectivity profiles vary substantially between individuals, acting as an identifying fingerprint (Mira-Dominguez *et al.*, 2014; Finn *et al.*, 2015) that is stable over long periods of time (Horien *et al.*, 2019). Conversely, it is well-known that physiological processes (Pitzalis *et al.*, 1996; Batchvarov *et al.*, 2002; Reland *et al.*, 2005; Pinna *et al.*, 2007; Malik *et al.*, 2008; Power *et al.*, 2020) and head motion (van Dijk, Sabuncu and Buckner, 2012; Zeng *et al.*, 2014) are likewise highly subject-specific. Furthermore, it has been shown that the intraclass correlation values of functional connections associated to test-retest reliability across sessions within-subject is reduced when a relatively aggressive pipeline is used (Birn *et al.*, 2014; Parkes *et al.*, 2018), suggesting that artifacts have high subject specificity. Therefore, inter-individual differences in physiological processes and head motion may contribute to subject discrimination.

In the present work, we investigate the signatures of nuisance processes and head motion on estimates of static and time-varying FC at rest, based on 3T fMRI data from the Human Connectome Project (HCP). To quantify the contributions of physiological processes and head motion on FC, we employ model-based techniques with externally recorded physiological measurements, and subsequently generate nuisance datasets that only contain non-neural fluctuations. Using these datasets, we provide a comprehensive examination of the regional variability of the impact of these nuisance processes on the BOLD signal, as well as an investigation of the group consistency and inter-individual differences of their characteristic signature on FC. We further evaluate several fMRI preprocessing strategies to assess which techniques better remove the physiological signatures. Finally, we investigate the potential effect of physiological processes on individual discriminability in the context of connectome fingerprinting.

Using this approach, we show that low-frequency physiological processes and motion have the largest impact on FC measures, and the results highlight which functional connections are more prone to exhibit biases. Furthermore, our findings suggest that the recurrent whole-brain connectivity patterns observed in time-varying FC can be partly attributed to systemic low frequency fluctuations and head motion. Finally, we found that connectome fingerprinting accuracies are higher when non-neural confounds are reduced, suggesting a neural origin underpinning these observations.

The codes employed to carry out the analyses detailed in this study are publicly available and can be found on https://github.com/axifra/Nuisance_signatures_FC.

2 Materials and Methods

2.1 Human Connectome Project (HCP) dataset

The resting-state fMRI data analysed in this study are from the S1200 release of the 3T HCP dataset (Smith *et al.*, 2013; Van Essen *et al.*, 2013), which consists of young, healthy twins and siblings (age range: 22-36 years). The HCP dataset includes, among others, resting-state data acquired on two different days, during which subjects were instructed to keep their eyes open and fixated on a cross-hair. Each day included two consecutive 15-min resting-state runs, acquired with left-to-right (LR) and right-to-left (RL) phase encoding direction. During each fMRI run, 1200 frames were acquired using a gradient-echo echo-planar imaging (EPI) sequence with a multiband factor of 8, spatial resolution of 2 mm isotropic voxels, and a TR of 0.72 s. Further details of the data acquisition parameters can be found in previous publications (Van Essen *et al.*, 2012; Smith *et al.*, 2013). Concurrently with fMRI images, cardiac and respiratory signals were measured using a standard Siemens pulse oximeter placed on the fingertip and a breathing belt placed around the chest, with a 400 Hz sampling rate.

We only considered subjects who had available data from all 4 runs, and excluded subjects based on the quality of the physiological recordings (see section 2.2.1 below for details). Pulse oximeter and respiratory belt signals from ~1000 subjects were first visually inspected to determine their quality, since their traces are often not good enough for reliable peak detection (Power, 2019). The selection process resulted in a final dataset with 392 subjects (ID numbers provided in Supp. Material).

2.2 Preprocessing

2.2.1 Preprocessing of physiological recordings

After selecting subjects with good quality traces, the pulse wave was processed to automatically detect beat-to-beat intervals (RR), and the HR signal was further computed as the inverse of the time differences between pairs of adjacent peaks and scaled to beats-per-minute (bpm). HR traces were visually checked to ensure that outliers and abnormalities were not present. An outlier replacement filter was used to eliminate spurious changes in HR when these changes were found to be due to sporadic noisy cardiac measurements (for more details see Supp. Figs. 1 and 2 from (Kassinopoulos and Mitsis, 2019a)). We also excluded subjects with a HR of exactly 48 bpm and lack of heartbeat interval variability, as they have been pointed out as outliers in recent studies (Orban *et al.*, 2019; Valenza *et al.*, 2019). The signal from the breathing belt was detrended linearly, visually inspected and corrected for outliers using a replacement filter. Subsequently, it was low-pass filtered at 5 Hz and z-scored. The respiratory flow (RF), proposed in (Kassinopoulos and Mitsis, 2019a) as a robust measure of the absolute flow of inhalation and exhalation of a subject at each time point, was then extracted by applying further smoothing on the breathing signal (moving

average filter of 1.5 sec window) and, subsequently, computing the square of the derivative of the smoothed breathing signal. Finally, HR and RF time-series were re-sampled to 10 Hz.

An example code (Preprocess_Phys.m) showing the detailed specifications of the algorithms used during the preprocessing of the physiological signals is available on https://github.com/mkassinopoulos/PRF_estimation/.

2.2.2 Preprocessing of fMRI data: assessing the impact of nuisance correction strategies

From the HCP database we downloaded the minimally preprocessed data described in (Glasser *et al.*, 2013) and the FIX-denoised data, both in volume and surface space. Briefly, the minimal preprocessing pipeline included removal of spatial distortion, motion correction via volume re-alignment, registration to the structural image, bias-field correction, 4D image intensity normalization by a global mean, brain masking, and non-linear registration to MNI space. Further steps to obtain surface data were volume to surface projection, multimodal inter-subject alignment of the cortical surface data (Robinson *et al.*, 2014), and 2 mm (FWHM) surface-constrained smoothing. Additional steps following minimal preprocessing to obtain the FIX-denoised data were de-trending using a mild high-pass filter (2000 s), head motion correction via 24 parameter regression, and denoising via spatial ICA followed by an automated component classifier (FMRIB's ICA-based X-noiseifier, FIX) (Griffanti *et al.*, 2014; Salimi-Khorshidi *et al.*, 2014). Minimal spatial smoothing (FWHM = 4 mm) was applied to the downloaded minimally preprocessed and FIX-denoised volumetric data. Both minimally preprocessed and FIX-denoised data were parcellated with the Gordon atlas across 333 regions of interest (ROIs) (Gordon *et al.*, 2016) and the Seitzman atlas across 300 ROIs (Seitzman, Gratton, Marek, *et al.*, 2019), using the volume and surface space data, respectively. ROIs that did not belong to a brain network were disregarded, hence a total of 286 ROIs (Gordon atlas) and 285 ROIs (Seitzman atlas) were used for further analyses. The main differences between these two brain parcellations, apart from being computed on the surface and volume space, respectively, are that the ROIs in the Gordon atlas do not have the same size, whereas in the Seitzman atlas the ROIs are all spheres of 8 mm diameter, and that the Gordon atlas only includes cortical regions, whereas the Seitzman atlas includes cortical and subcortical regions. The results from the Gordon atlas are presented in the main manuscript whereas the results from the Seitzman atlas can be found in the Supplementary Material (**Supp. Fig. 8**, **Supp. Fig. 9**, **Supp. Fig. 10**). Further, the parcellated data were high-pass filtered at 0.01 Hz.

Apart from the FIX-denoising strategy, several other data-driven preprocessing techniques were evaluated here to assess how well they remove physiological and motion-driven confounds (**Table 1**). We chose pipelines that had been used in the landmark FC studies of (Finn *et al.*, 2015) and (Laumann *et al.*, 2017). These were denoted as

Table 1. Preprocessing strategies examined. All strategies were evaluated with and without global signal regression (GSR).

Preprocessing strategy	Acronym	Regressors included
Minimally preprocessed HCP data	Minprep	-
FIX-denoised HCP data	FIX	-
Pipeline used in Finn et al. (2015), *Nature Neuroscience*	MildA	Mean time-series of the white matter and CSF voxels (2); realignment parameters and their first derivatives (12)
Pipeline used in Laumann et al. (2017), *Cerebral Cortex*	MildB	Mean time-series of the white matter and CSF voxels and their derivatives (4); realignment parameters and their first derivatives, quadratic terms, and squares of derivatives (24)
Pipeline proposed by Kassinopoulos & Mitsis (2019b), *bioRxiv*	WM_{50}	50 PCA components from white matter voxels
	WM_{200}	200 PCA components from white matter voxels

"mild" pipelines, since they regress out considerably fewer components compared to FIX. Further, we also included two more "aggressive" pipelines that were found to outperform previously proposed techniques (Kassinopoulos and Mitsis, 2019b). The nuisance regression was performed after the minimally preprocessed data had been parcellated to reduce computational time. All preprocessing strategies were evaluated with and without global signal regression (GSR), since whether GSR should be performed or not is somewhat controversial (Liu, Nalci and Falahpour, 2017; Murphy and Fox, 2017). In addition, to ease the comparison between preprocessing strategies, the minimally preprocessed data were also evaluated yielding in total 12 preprocessing strategies. The regressors included in each preprocessing strategy can be found in **Table 1**. Note that for the pipeline from (Laumann *et al.*, 2017) the global signal's derivative was also regressed out. The global signal for the surface and volumetric data was computed as the average fMRI timeseries across vertices and the whole brain, respectively.

2.3 Nuisance processes evaluated

The following four nuisance processes were evaluated (**Table 2**):

a. **Systemic low frequency oscillations (SLFOs):** SLFOs refer to non-neuronal global BOLD fluctuations. Major sources of SLFOs are spontaneous fluctuations in the rate or depth of breathing (Birn *et al.*, 2006), which influence the concentration of CO_2 in the blood, a potent vasodilator, altering CBF and thus BOLD signals (Wise *et al.*, 2004; Birn *et al.*, 2008; Birn, Murphy and Bandettini, 2008; Chang and Glover, 2009b; Prokopiou *et al.*, 2019), and fluctuations in heart rate (Shmueli *et al.*, 2007; Chang, Cunningham and Glover, 2009). Importantly, SLFOs seem to be the main physiological noise source in BOLD fMRI rather than high frequency cardiac pulsatility and breathing motion artifacts (Tong and Frederick, 2014; Tong, Hocke and Frederick, 2019). In this study, SLFOs were modelled following a framework proposed in our previous work (Kassinopoulos and Mitsis, 2019a), scripts available on https://github.com/mkassinopoulos/PRF_estimation/. Briefly, the extracted

HR and RF signals were fed into an algorithm that estimated scan-specific physiological response functions (PRFs). This algorithm estimates PRF curves so that the convolution of HR and RF with their corresponding PRFs fits as well as possible the global signal of the same scan while ensuring that the shapes of the PRF curves are physiologically plausible. The HR and RF signals were then convolved with their respective PRFs and added together in order to yield a time-series that reflects SLFOs (**Supp. Fig. 1**). This time-series is used in the current study as the physiological regressor related to SLFOs.

b. Cardiac pulsatility: Pulsatility of blood flow in the brain can cause appreciable modulations of the BOLD signal (Noll and Schneider, 1994), which tend to be rather localized along the vertebrobasilar arterial system and the sigmoid transverse and superior sagittal sinuses (Dagli, Ingeholm and Haxby, 1999; Kassinopoulos and Mitsis, 2019a). We modelled fluctuations induced by cardiac pulsatility using 6 regressors obtained with 3rd order RETROICOR (Glover, Li and Ress, 2000) using the pulse oximeter signal of each scan.

c. Breathing Motion: Chest movements during the breathing cycle generate head motion in the form of head nodding by mechanical linkage through the neck, but also factitious motion (also known as pseudomotion) through small perturbations of the B_0 magnetic field caused by changes in abdominal volume when air enters the lungs (Raj, Anderson and Gore, 2001; Van de Moortele *et al.*, 2002; Power *et al.*, 2019). We modelled breathing-induced fluctuations using 6 regressors obtained with 3rd order RETROICOR (Glover, Li and Ress, 2000) based on the respiratory signal of each scan.

d. **Head motion:** Subject motion produces substantial signal disruptions in fMRI studies (Friston *et al.*, 1996; Power *et al.*, 2012) and is a major confound when evaluating connectivity differences between groups with dissimilar tendencies for motion (Satterthwaite *et al.*, 2012; van Dijk, Sabuncu and Buckner, 2012; Makowski, Lepage and Evans, 2019). We quantified head motion using the six realignment parameters as well as their temporal first derivatives provided by HCP. The six physiological regressors related to breathing motion were regressed out from the realignment parameters and their derivatives, since true and factitious motion due to breathing is reflected in the realignment parameters (Fair *et al.*, 2019).

Table 2. Nuisance processes examined.

	SLFOs	Cardiac pulsatility	Breathing motion	Head motion
Recordings	Pulse oximeter, breathing belt, fMRI global signal	Pulse oximeter	Breathing belt	fMRI
Signals employed	Heart rate, respiratory flow, global signal	Cardiac cycle	Breathing cycle	Realignment parameters and derivatives
Model	Kassinopoulos & Mitsis (2019a), *NeuroImage*	3rd order RETROICOR Glover et al. (2000), *NeuroImage*	3rd order RETROICOR Glover et al. (2000), *NeuroImage*	-
Number of regressors	1	6	6	12

All nuisance regressors were high-pass filtered at 0.01 Hz to ensure similar spectral content with the fMRI data and thus avoid reintroduction of nuisance-related variation (Hallquist, Hwang and Luna, 2013; Bright, Tench and Murphy, 2017). The regressors were then normalized to zero mean and unit variance. **Supp. Fig. 2** demonstrates the spectral content of each nuisance process, as well as the effect of regressing out breathing motion from the realignment parameters.

2.4 Isolation of nuisance fluctuations from fMRI data

We propose a framework to isolate nuisance fluctuations for each of the aforementioned processes, which reflects the physiologically-driven fluctuations and head motion artifacts observed in the fMRI data (**Figure 1**). Similar methodology was used in (Bright and Murphy, 2015) to investigate whether preprocessing strategies remove variance associated to resting-state networks.

Initially, the contribution of each nuisance process on the ROI time-series was quantified using a generalised linear model, formulated as:

$$y(t) = \beta_0 + \beta_{SLFOs} x_{SLFOs}(t) + \boldsymbol{\beta}_{CP}\mathbf{x}_{CP}(t) + \boldsymbol{\beta}_{BM}\mathbf{x}_{BM}(t) + \boldsymbol{\beta}_{HM}\mathbf{x}_{HM}(t) + \varepsilon(t) \tag{1}$$

$$\boldsymbol{\beta}_{CP} = [\beta_{CP}^1 \quad \cdots \quad \beta_{CP}^6],\ \boldsymbol{\beta}_{BM} = [\beta_{BM}^1 \quad \cdots \quad \beta_{BM}^6],\ \boldsymbol{\beta}_{HM} = [\beta_{HM}^1 \quad \cdots \quad \beta_{HM}^{12}]$$

$$\mathbf{x}_{CP}(t) = \begin{bmatrix} x_{CP}^1(t) \\ \vdots \\ x_{CP}^6(t) \end{bmatrix},\ \mathbf{x}_{BM}(t) = \begin{bmatrix} x_{BM}^1(t) \\ \vdots \\ x_{BM}^6(t) \end{bmatrix},\ \mathbf{x}_{HM}(t) = \begin{bmatrix} x_{HM}^1(t) \\ \vdots \\ x_{HM}^{12}(t) \end{bmatrix}$$

where y is an ROI time-series from the minimally preprocessed data, x_{SLFOs} is the physiological regressor modeling SLFOs, $\mathbf{x}_{CP}(t)$ are the 6 physiological regressors modeling cardiac pulsatility, $\mathbf{x}_{BM}(t)$ are the 6 physiological regressors modeling breathing motion, $\mathbf{x}_{HM}(t)$ are the 12 regressors modeling head motion, the values $\{\beta_0, \beta_{SLFOs}, \boldsymbol{\beta}_{CP}, \boldsymbol{\beta}_{BM}, \boldsymbol{\beta}_{HM}\}$ represent the parameters to be estimated, and ε is the error (or residual). As can be seen, all four nuisance processes (25 regressors in total) were included simultaneously in the regression to model the fluctuations at a specific ROI.

For each nuisance process, the estimated $\hat{\beta}$ values were multiplied by their corresponding regressors and added together to obtain the fluctuations of the nuisance process of interest ($\hat{y}_{NPI}(t)$) at a specific ROI, and a "clean" time-series was calculated via removal of all other nuisance processes ($\hat{y}_{NPI+Neur}(t)$), as follows:

SLFOs:

$$\hat{y}_{NPI}(t) = \hat{\beta}_{SLFOs} x_{SLFOs}(t) \tag{2}$$

$$\hat{y}_{NPI+Neur}(t) = y(t) - \hat{\beta}_0 - \widehat{\boldsymbol{\beta}}_{CP}\mathbf{x}_{CP}(t) - \widehat{\boldsymbol{\beta}}_{BM}\mathbf{x}_{BM}(t) - \widehat{\boldsymbol{\beta}}_{HM}\mathbf{x}_{HM}(t) \tag{3}$$

Cardiac pulsatility:

$$\hat{y}_{NPI}(t) = \widehat{\boldsymbol{\beta}}_{CP}\mathbf{x}_{CP}(t) \tag{4}$$

$$\hat{y}_{NPI+Neur}(t) = y(t) - \hat{\beta}_0 - \hat{\beta}_{SLFOs} x_{SLFOs}(t) - \widehat{\boldsymbol{\beta}}_{BM} \mathbf{x}_{BM}(t) - \widehat{\boldsymbol{\beta}}_{HM} \mathbf{x}_{HM}(t) \quad (5)$$

Breathing motion:

$$\hat{y}_{NPI}(t) = \widehat{\boldsymbol{\beta}}_{BM} \mathbf{x}_{BM}(t) \quad (6)$$

$$\hat{y}_{NPI+Neur}(t) = y(t) - \hat{\beta}_0 - \hat{\beta}_{SLFOs} x_{SLFOs}(t) - \widehat{\boldsymbol{\beta}}_{CP} \mathbf{x}_{CP}(t) - \widehat{\boldsymbol{\beta}}_{HM} \mathbf{x}_{HM}(t) \quad (7)$$

Head motion:

$$\hat{y}_{NPI}(t) = \widehat{\boldsymbol{\beta}}_{HM} \mathbf{x}_{HM}(t) \quad (8)$$

$$\hat{y}_{NPI+Neur}(t) = y(t) - \hat{\beta}_0 - \hat{\beta}_{SLFOs} x_{SLFOs}(t) - \widehat{\boldsymbol{\beta}}_{CP} \mathbf{x}_{CP}(t) - \widehat{\boldsymbol{\beta}}_{BM} \mathbf{x}_{BM}(t) \quad (9)$$

In this manner, we generated "cleaned" ROI time-series ($\hat{y}_{NPI+Neur}(t)$) in which all considered noisy fluctuations were removed except the ones from the specific nuisance process being evaluated. The next step was to quantify the contributions of this nuisance process to the remaining ROI's fluctuations. To achieve this, the estimated nuisance signal was correlated to the "clean" ROI time-series:

$$r_{nuis} = corr(\hat{y}_{NPI}(t), \hat{y}_{NPI+Neur}(t)) \quad (10)$$

Then, the estimated nuisance signal was subtracted from the "clean" ROI time-series to obtain what is usually considered the "neural" time-series. This time-series was correlated to the "clean" time-series to quantify the contribution of the "neural" variations to the ROI's fluctuations:

$$\hat{y}_{Neur}(t) = \hat{y}_{NPI+Neur}(t) - \hat{y}_{NPI}(t) \quad (11)$$

$$r_{neur} = corr(\hat{y}_{Neur}(t), \hat{y}_{NPI+Neur}(t)) \quad (12)$$

Afterwards, nuisance datasets for each nuisance process were created by scaling the estimated nuisance signal at each ROI with its corresponding r_{nuis} and adding Gaussian random signals ($\xi(t)$) scaled with r_{neur}. This is expressed as,

$$y_{Nuis}(t) = r_{nuis}\, Z[\hat{y}_{NPI}(t)] + r_{neur}\, Z[\xi(t)] \quad (13)$$

where $Z[\cdot]$ denotes the normalization of a time series to zero mean and unit variance.

Thus, this framework generated four synthetic nuisance datasets that contained the isolated fluctuations from each of the nuisance processes evaluated. In a sense, the ROI's time-series in each nuisance dataset are equivalent to the term $\hat{y}_{NPI+Neur}(t)$ with the "neural" fluctuations replaced by random signals in order to characterize the signature of the nuisance processes on FC without the presence of neurally-related signals, while maintaining the ratio of noise and "neural" signal intact. Note that if the nuisance datasets consisted solely of artifactual fluctuations without the random signals added, this would result in overestimation of the correlation attributed to nuisance processes that could be found in real fMRI data. This can be easily understood in the case of two ROI time-series that are weakly driven by SLFOs. As the contribution of this nuisance process to the ROI's time-series would be small, the parameter $\hat{\beta}_{SLFOs}$ in Eq. 2 for both ROIs would be relatively small as well. However, without the addition of random

signals, the correlation of the time-series $\hat{y}_{NPI}$ associated with these two ROIs would be 1.00 (or -1.00 depending on the signs of the beta parameters) as Pearson's correlation is a metric blinded to the variance of the signals, thereby overestimating the contribution of SLFOs to the FC between those ROIs.

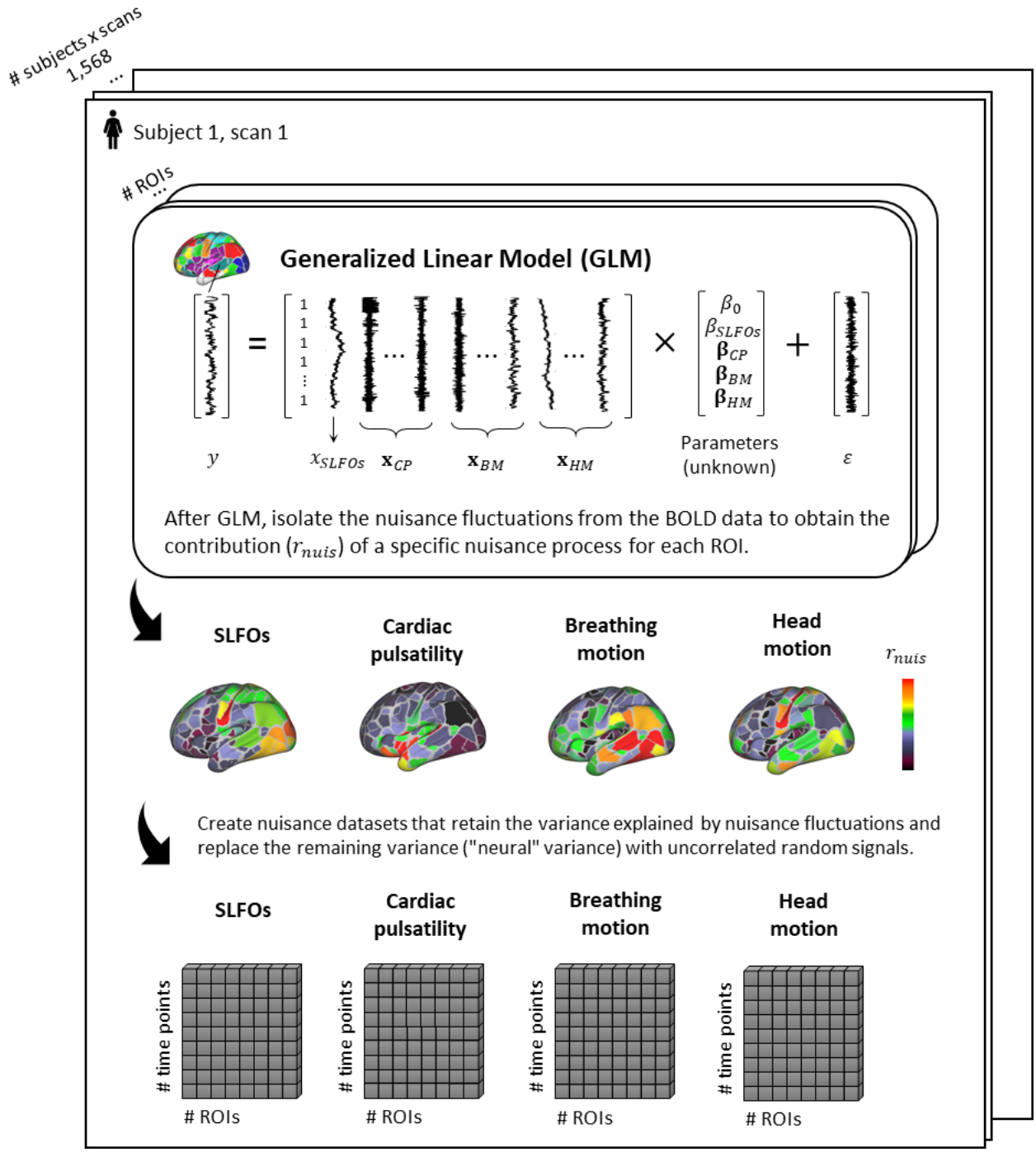

Figure 1. Graphical summary of the proposed framework to isolate the fluctuations for each physiological process and create four nuisance datasets for each subject. SLFOs = Systemic low frequency oscillations, CP = cardiac pulsatility, BM = Breathing motion, HM = Head motion.

2.5 Estimation of static and time-varying functional connectivity (FC)

Using the pre-processed fMRI data from each of the 12 pipelines (see section 2.2.2), henceforth called "neural" datasets, and the 4 nuisance datasets, we performed Pearson correlation analyses between brain regions over the whole scan (static FC) and within sliding-windows (time-varying FC). To quantify time-varying FC, the entire scan was split up into 62 sliding windows of 43.2 sec (60 samples) duration, with 70% overlap in time. Subsequently, for each scan, the functional connectivity dynamics (FCD) matrix (Hansen *et al.*, 2015) was computed, which is a symmetric matrix whose entries (i, j) correspond to the Pearson correlations between the upper triangular elements of the FC matrices at windows i and j. The size of the FCD matrix was W×W where W is the number of windows (62). Thus, while the static FC matrix characterizes the spatial structure of resting activity, the FCD matrix captures the temporal evolution of those connectome correlations.

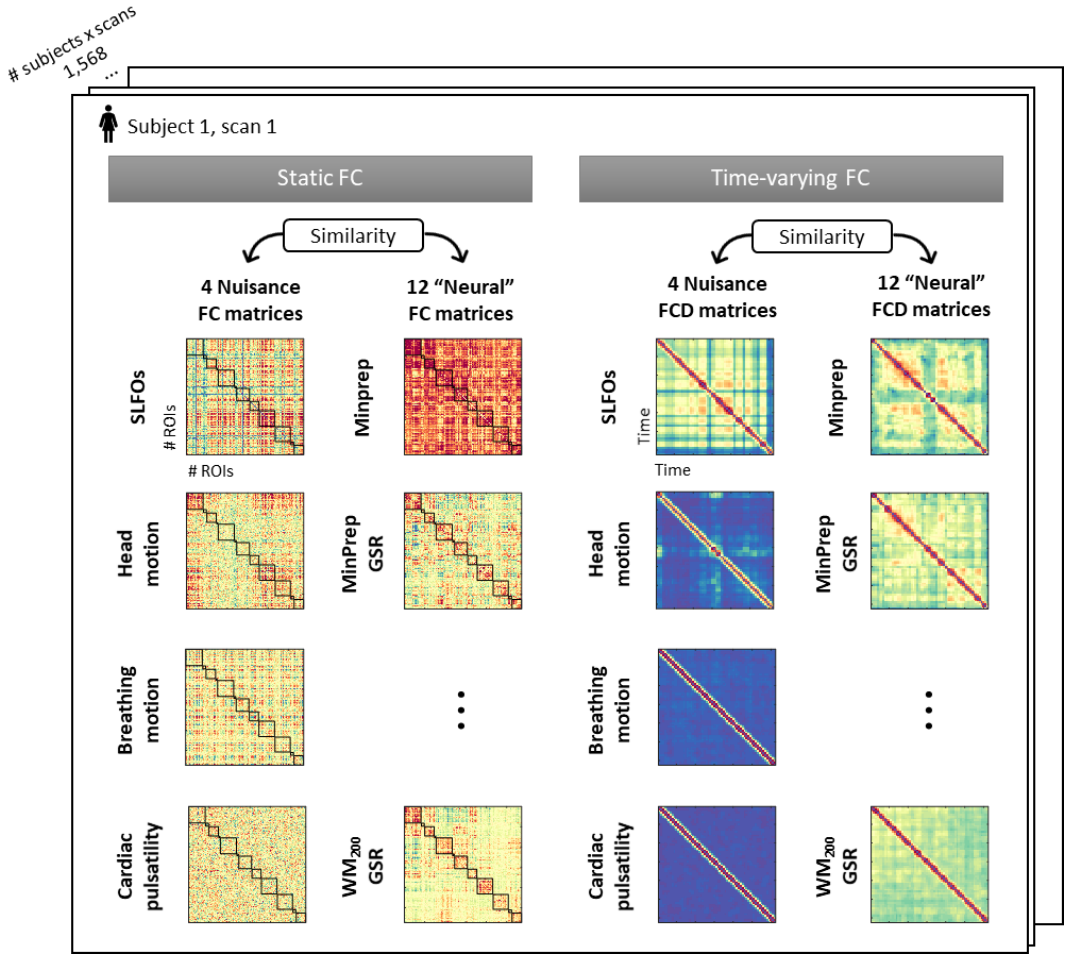

Figure 2. Illustration of the 32 connectivity matrices computed per scan. For both static and time-varying FC analyses, 4 nuisance connectivity matrices were computed using the generated nuisance datasets, as well as 12 "neural" connectivity matrices corresponding to the 12 pre-processing strategies evaluated (note that each of the 6 strategies listed in Table 1 was assessed with and without GSR). Static FC matrices were computed as the correlation across brain regions using the whole scan. Time-varying FC analysis constructed time-resolved connectivity matrices as the correlation between static FC matrices within sliding windows, known as functional connectivity dynamics (FCD) matrices (Hansen et al. 2015).

The analyses resulted in 32 matrices for each subject (**Figure 2**): 4 static FC and 4 FCD nuisance matrices (one for each physiological process considered), and 12 static FC and 12 FCD "neural" matrices (one for each preprocessing strategy evaluated). To quantify the influence of the nuisance processes on static FC and FCD for each preprocessing strategy, similarities between pairs of nuisance and "neural" matrices were evaluated by correlating their upper triangular values. Note that for the FCD matrices, upper triangular elements corresponding to the correlation between overlapping windows were disregarded because of high autocorrelation (see block diagonal in **Figure 2**). All correlation values were Fisher z transformed.

2.6 Connectome-based identification of individual subjects

We applied a connectome-based identification of individual subjects on the static FC matrices in order to investigate the potential effect of "nuisance fingerprints" on the degree of subject specificity in individual FC metrics. The identification procedure, known as connectome fingerprinting, has been described in detail previously (Finn *et al.*, 2015). Briefly, a database is first created consisting of all subjects' FC matrices from a particular resting-state scan (**Supp. Fig. 3B**). An FC matrix from a specific subject and different resting-state scan is then selected and denoted as the target ($Subj_x$). Pearson correlation coefficients ($r_1, \dots, r_N$) are computed between the upper triangular values of the target FC matrix and all the FC matrices in the database. If the highest correlation coefficient corresponds to a pair of FC matrices from the same subject, a successful identification is noted ($ID_{Subj_x} = 1$); otherwise, it is marked as an incorrect identification ($ID_{Subj_x} = 0$). The identification test is repeated such that each subject serves as the target subject once, and then the ID values are averaged across subjects to obtain the identification accuracy of the database-target pair. This process is repeated until tests have been performed between all scanning sessions. In total, 12 database-target combinations were computed (**Supp. Fig. 3A**). Identification was performed using the whole brain connectivity matrix as well as based on edges from within and between networks. In the latter case, networks containing less than 10 ROIs were excluded from the analysis.

The connectome fingerprinting analysis was performed independently for each physiological process, as well as for each preprocessing strategy, using the generated FC matrices (**Figure 2**). This analysis was only performed on static FC matrices and not time-varying FC matrices because recurrent patterns of connectivity observed in the FCD matrices are not expected to occur at similar time instances between scans.

2.7 Statistics

To assess the significance of the results, surrogate nuisance datasets were generated via inter-subject surrogates (Lancaster *et al.*, 2018), using fMRI data recorded from one subject's scan and physiological signals recorded from a different subject's scan (in the case of the head motion dataset, volume realignment parameters were employed).

This procedure was performed for all 1,568 scans, creating a surrogate dataset for each of the four examined physiological processes with the same dimensions as the evaluated datasets. Note that when creating each surrogate dataset, only the nuisance process being examined is replaced by signals from a different subject, whereas all other nuisance regressors remain the same. The same analyses described before were repeated using these surrogate datasets, generating a chance distribution against which the results were compared. Thus, the significance of the contributions of each nuisance process to the BOLD fluctuations were tested against the contributions found using the surrogate data (two-sample t-test, $p<0.05$, Bonferroni corrected), and the similarity between the nuisance and "neural" FC matrices was compared against the similarity obtained using surrogate nuisance FC matrices.

To assess the significance of the fingerprinting analysis, we performed nonparametric permutation testing as in (Finn *et al.*, 2015). Briefly, the described fingerprinting analysis was repeated for all scans and database-target combinations, but at the identification test the subject identity in the database set was permuted. In this way, a "successful" identification was designated when the highest correlation coefficient was between the FC matrices of two different subjects. As expected, for all the nuisance and "neural" datasets, the identification accuracy estimated with nonparametric permutation testing was around 0.3% which corresponds to the probability of selecting a specific subject from a group of 392 subjects when the subject is selected at random.

3 Results

3.1 Contributions of nuisance processes on the BOLD signal

We examined regional differences in the influence of physiological processes and head motion on the BOLD signal. Scans with LR and RL phase encoding were examined separately as it had been suggested that breathing motion artifacts vary across scans with different phase encoding directions (Raj, Anderson and Gore, 2001), and it is not clear whether other processes such as head motion demonstrate similar dependence. The contributions of each nuisance process on BOLD fluctuations were quantified as the correlation between the nuisance fluctuations of the process in question and the BOLD fluctuations "cleaned" of all other nuisance fluctuations (denoted as r_{nuis} in the Methods section, see also **Figure 1**). We computed these contributions for each scan and then tested for the presence of consistent patterns across scans with the same phase encoding direction (significance testing using inter-subject surrogates, two-sample t-test, $p<0.05$, Bonferroni corrected).

The results showed distinct regional variations for each of the nuisance processes. SLFOs mostly affected sensory regions including visual cortex and somatosensory cortex (particularly of the face) (**Figure 3A**). Phase encoding did not seem to modulate the magnitude of the SLFOs contributions on the BOLD signal (**Figure 3A**). Head motion exhibited the largest effect in somatosensory and visual cortices (**Figure 3B**). Intriguingly, the effect in the visual cortex was highest in the right hemisphere for LR phase encoding, but highest in the left hemisphere for RL phase encoding **(Figure 3B**). Breathing motion effects were more pronounced in prefrontal, parietal and temporal brain regions (**Figure 3C**). Further, breathing motion had a much larger impact on the left hemisphere when the phase encoding was LR, whereas the reverse pattern was observed for RL phase encoding (**Figure 3C**). Cardiac pulsatility was highest in regions such as the visual and auditory cortices, as well as the insular cortex (**Figure 3D**).

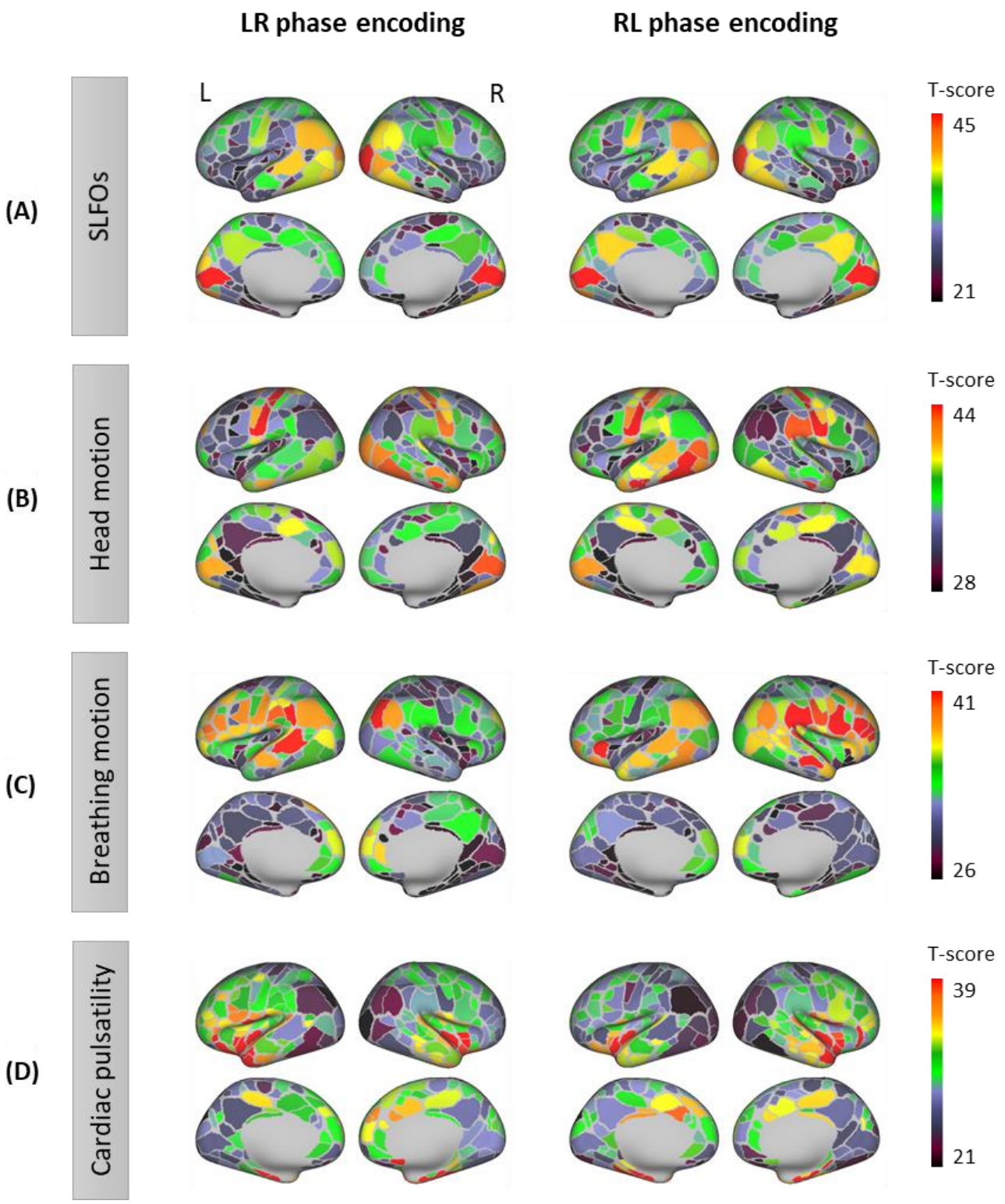

Figure 3. T-score maps of the correlation of each nuisance process with the fMRI fluctuations (Minprep data) for **(A)** SLFOs, **(B)** head motion, **(C)** breathing motion, and **(D)** cardiac pulsatility, computed at each parcel of the Gordon atlas (two-sample t-test against the surrogate data, $p<0.05$, Bonferroni corrected). The t-tests were calculated for each phase encoding separately. The physiological fluctuations were obtained from externally recorded processes.

3.2 Physiological and head motion signatures on static FC

We computed connectivity matrices for each scan using the nuisance datasets independently. The group-averaged results across all 1,568 scans revealed consistent signatures for SLFOs, head motion and breathing motion (**Figure 4A-C**). SLFOs exhibited strong positive correlations in all the edges of the FC matrix, but particularly higher in edges within the visual network and between the visual network and the rest of brain networks (**Figure 4A**). Head motion mainly influenced functional connections within the visual and sensorimotor networks, as well as edges within the DMN (**Figure 4B**). Note that even though areas in both the visual and sensorimotor network were influenced by motion artifacts (**Figure 3B**), we did not observe strong correlations between areas of the two aforementioned networks. This is not surprising as a different linear combination of nuisance regressors (in this case head motion regressors) may be associated with two areas affected by a nuisance process and, thus, the correlation of their nuisance fluctuations can in principle be around zero. Breathing motion exhibited an intriguing chess-like pattern, with both positive and negative correlations (**Figure 4C**, lower triangular matrix). We then reordered the ROIs with respect to the hemisphere they belong to, which revealed that positive correlations were mostly confined within ROIs of the same hemisphere, whereas correlations between hemispheres were close to zero or even negative (**Figure 4C**, upper triangular matrix). Even when scans with LR and RL phase encoding were averaged separately, both hemispheres exhibited increased within-hemisphere connectivity (**Supp. Fig. 4C**). Nonetheless, the signature of breathing motion had clear differences between phase encoding directions, whereas all other nuisance processes did not show perceivable differences (**Supp. Fig. 4**). Finally, cardiac pulsatility did not show a characteristic spatial pattern and the group-averaged correlations were quite small, suggesting that cardiac pulsatility does not affect static FC in a systematic manner across subjects (**Figure 4D**).

3.3 Capability of preprocessing strategies to remove the nuisance signatures on static FC at the individual level

To examine the capability of various preprocessing strategies to reduce the bias introduced by physiological processes and head motion on static FC, we computed the similarity of the nuisance and "neural" FC matrices at the individual level. A distribution of the similarity values, in this case Pearson's correlation coefficients, is shown in **Figure 4E-H** for each preprocessing strategy and nuisance process. We found that SLFOs, head motion and breathing motion were the processes that had the strongest influence on static FC, based on the similarity of their signatures with the "neural" signature from the Minprep data (**Figure 4E-H**).

The signature induced by SLFOs remained after the MildA, MildB and FIX pipelines were applied, but was greatly reduced by the WM_{50} and WM_{200} strategies (**Figure 4E**). The observation that FIX, even though is quite an aggressive preprocessing strategy, was unable to remove most of the SLFOs is consistent with recent studies

showing that global artifactual fluctuations are still prominent after FIX denoising (Burgess *et al.*, 2016; Power *et al.*, 2017, 2018; Glasser *et al.*, 2018; Kassinopoulos and Mitsis, 2019a). Notably, GSR seemed to be an effective technique to remove the physiological signature from SLFOs on static FC, albeit for some scans GSR appeared to introduce a negative correlation between the SLFOs and "neural" FC matrices (**Figure 4E**). This effect was greater if the global signal was computed across the whole brain in volumetric space compared to across vertices in surface space (**Supp. Fig. 5A**). The signature related to head motion was reduced with more aggressive preprocessing strategies, but none of the approaches examined completely eradicated the head motion signature on static FC (**Figure 4F**). GSR slightly reduced the similarity between the head motion signature and "neural" FC matrices. The signature induced by breathing motion was greatly reduced by all preprocessing strategies, and particularly by FIX denoising which almost reached chance level (**Figure 4G**). Still, none of the preprocessing strategies entirely eliminated the breathing motion signature on static FC. The bias introduced by cardiac pulsatility was overall small and effectively removed by FIX, WM_{50} and WM_{200} strategies in its entirety (**Figure 4H**). GSR did not have any effect on the removal of breathing motion and cardiac pulsatility signatures.

Finally, we also evaluated the addition of model-based nuisance regressors to the preprocessing strategies. Specifically, we added the physiological regressors used to model SLFOs (Kassinopoulos and Mitsis, 2019a), cardiac pulsatility and breathing motion (Glover, Li and Ress, 2000). We found that, when GSR was not performed, including the regressor that models SLFOs reduces the signature of SLFOs on static FC for all preprocessing strategies apart from WM_{50} and WM_{200}, even though the similarity remains well above chance levels (**Supp. Fig. 6A**). Including the RETROICOR regressors related to breathing motion appreciably reduced the breathing motion signature in the Minprep data, however all other preprocessing strategies remained the same (**Supp. Fig. 6C**). This suggests that the addition of RETROICOR regressors to tackle breathing motion is not worthwhile, since even conservative preprocessing strategies did not seem to benefit by it. On the contrary, including the RETROICOR regressors related to cardiac pulsatility completely removed this signature for the Minprep, MildA and MildB strategies (**Supp. Fig. 6D**), suggesting that conservative preprocessing strategies greatly benefit by adding these model-based regressors.

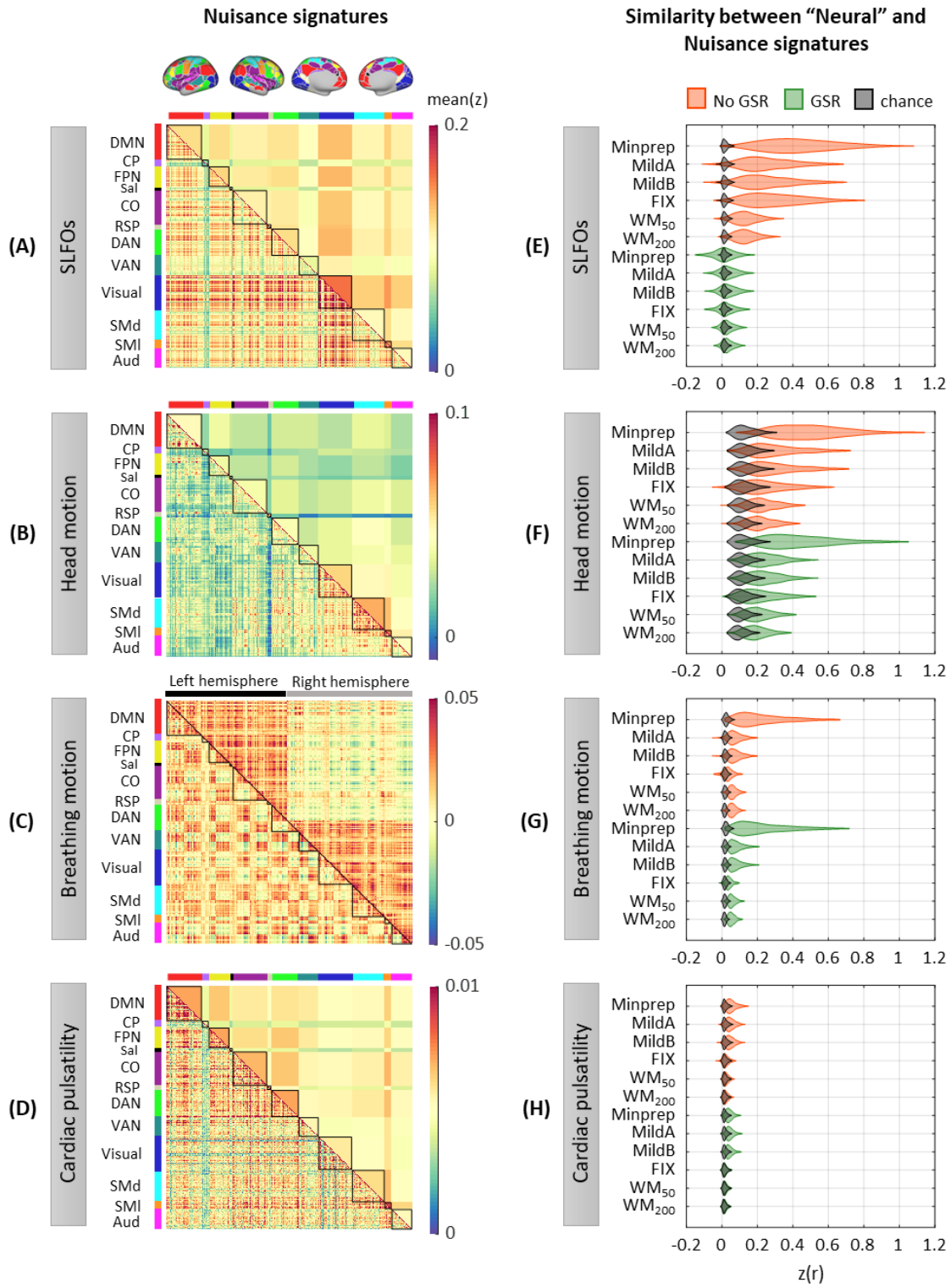

Figure 4. Static FC. (A-D) Group averaged nuisance FC matrices across all 1,568 scans for **(A)** SLFOs, **(B)** head motion, **(C)** breathing motion, and **(D)** cardiac pulsatility. **(E-H)** Distribution of Pearson correlation coefficients across all 1,568 scans between the "neural" FC matrix after each preprocessing pipeline and nuisance FC matrices associated to **(E)** SLFOs, **(F)** head motion, **(G)** breathing motion, and **(H)** cardiac pulsatility. Correlation values were Fisher z transformed. Note that correlation coefficients identified as outliers (> 3 SD) were disregarded.

3.4 Connectome-based identification of individual subjects

We next investigated how well FC matrices associated to physiological processes and head motion could identify an individual subject, and whether the accuracy of connectome-based fingerprinting was inflated by these nuisance processes.

We initially considered all the edges of the FC matrices for identification (Gordon atlas: 40,755 edges). Accuracy was above chance for nearly all database-target combinations for the nuisance processes, with rates up to 40% (**Figure 5A**). Breathing motion exhibited an intriguing bimodal distribution: database-target pairs that had the same phase encoding showed much higher identification rates than database-target pairs with different phase encodings, even if the latter were acquired the same day. This effect was also observed, although to a lesser extent, for cardiac pulsatility and head motion.

Identification accuracy was much higher for the "neural" datasets compared to the nuisance datasets, with rates ranging from 52% to 99% (**Figure 5B**). MildA, MildB and FIX techniques considerably improved the accuracy compared to the Minprep data, and WM_{50} and WM_{200} techniques significantly outperformed all preprocessing strategies. GSR considerably improved identification accuracy for the MildA, MildB and FIX strategies. Furthermore, we observed that for the Minprep data, database-target pairs from different days but with the same phase encoding showed identification rates as high as the ones from the same day but different phase encoding. In contrast, for all other preprocessing strategies the database-target pairs from the same day were always higher.

We then tested identification accuracy on the basis of within and between edges of specific functional networks to examine whether certain functional connections contributed more to individual subject discriminability than others. Results for the nuisance datasets are shown in **Figure 6A**, where it can be appreciated that nuisance processes exhibit a markedly lower identification accuracy when using specific edges compared to using all edges (**Figure 5A**). Furthermore, functional connections between networks seemed to contribute more to SLFOs' subject discriminability than connections within brain networks ($p<0.001$, Wilcoxon ranksum).

Regarding the "neural" datasets, we focused on the most aggressive strategies, namely FIX and WM_{200}. Networks of "top-down" control (FPN, CO, DAN, VAN), as well as DMN, showed higher identification accuracy compared to sensorimotor processing networks (Visual, SMd, Aud) in all preprocessing strategies (**Figure 6B**). These results indicate that FC patterns in higher-order association cortices ("top-down" control networks) tend to be distinctive within an individual, whereas primary sensory and motor regions (processing networks) tend to exhibit similar patterns between individuals, consistent with previous studies (Finn *et al.*, 2015; Gratton *et al.*, 2018; Horien *et al.*, 2019). We then tested for differences in identification accuracies between the Minprep data vs. FIX and WM_{200} data (**Figure 6C**, $p<0.05$, Bonferroni corrected, Wilcoxon ranksum). FIX denoising significantly increased the subject discriminability of connections within and between several top-down control networks, but significantly decreased the subject discriminability of connections between the FPN and SMd as well as FPN and Aud networks.

Conversely, WM_{200} denoising significantly increased the subject discriminability of connections within and between all top-down control networks, connections between the DAN and Visual network as well as the DAN and SMd network, and connections within the Visual and SMd networks.

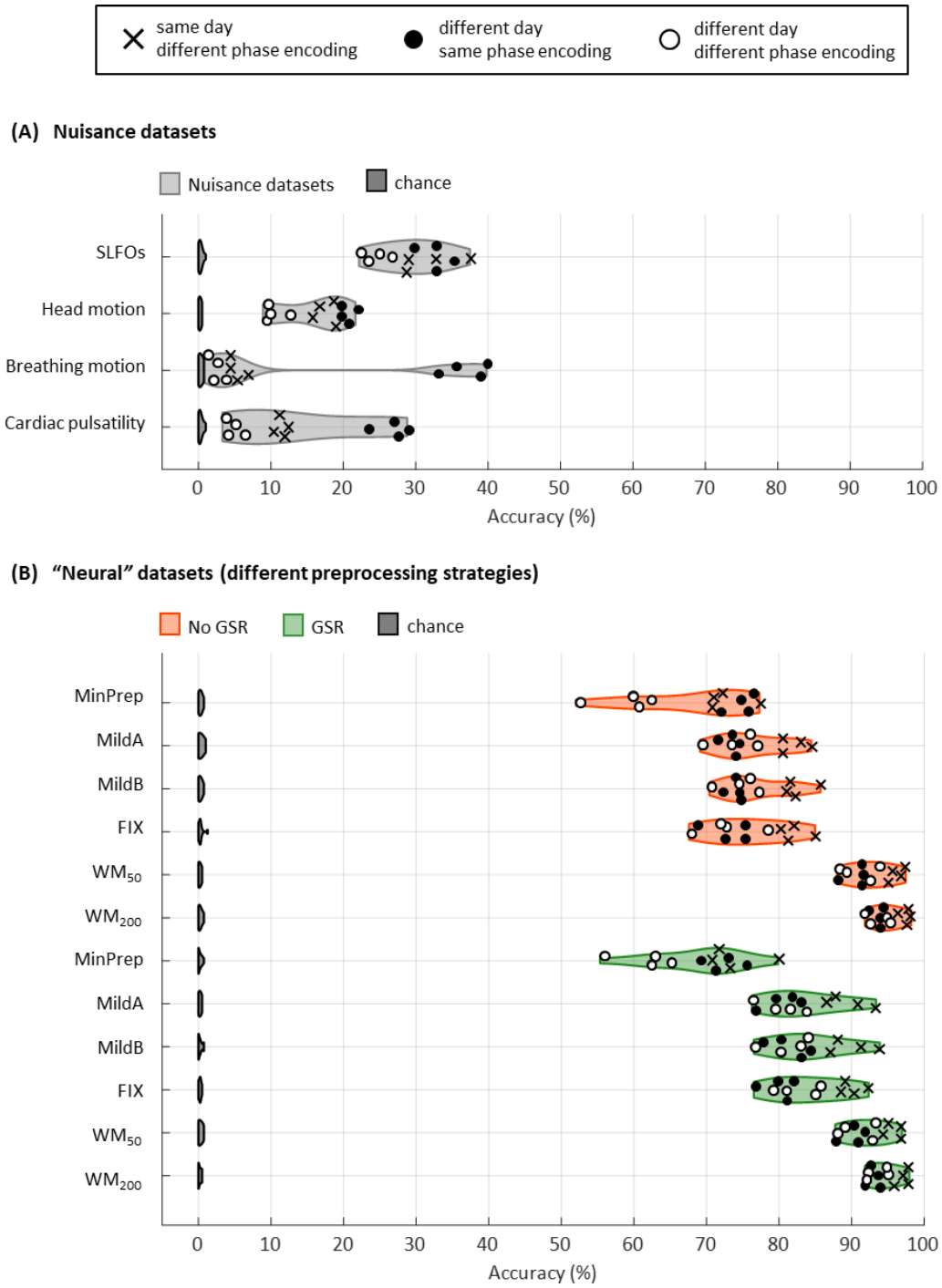

Figure 5. Connectome fingerprinting results. (A) Fingerprinting accuracy obtained using the static FC matrices from the generated nuisance datasets where non-neural fluctuations were isolated from the BOLD data. **(B)** Fingerprinting accuracy obtained using the static FC matrices generated from each of the preprocessing strategies evaluated. The pairs of resting-state scans are indicated with different symbols depending on whether they belong to the same or different day session, as well as whether they have the same phase encoding.

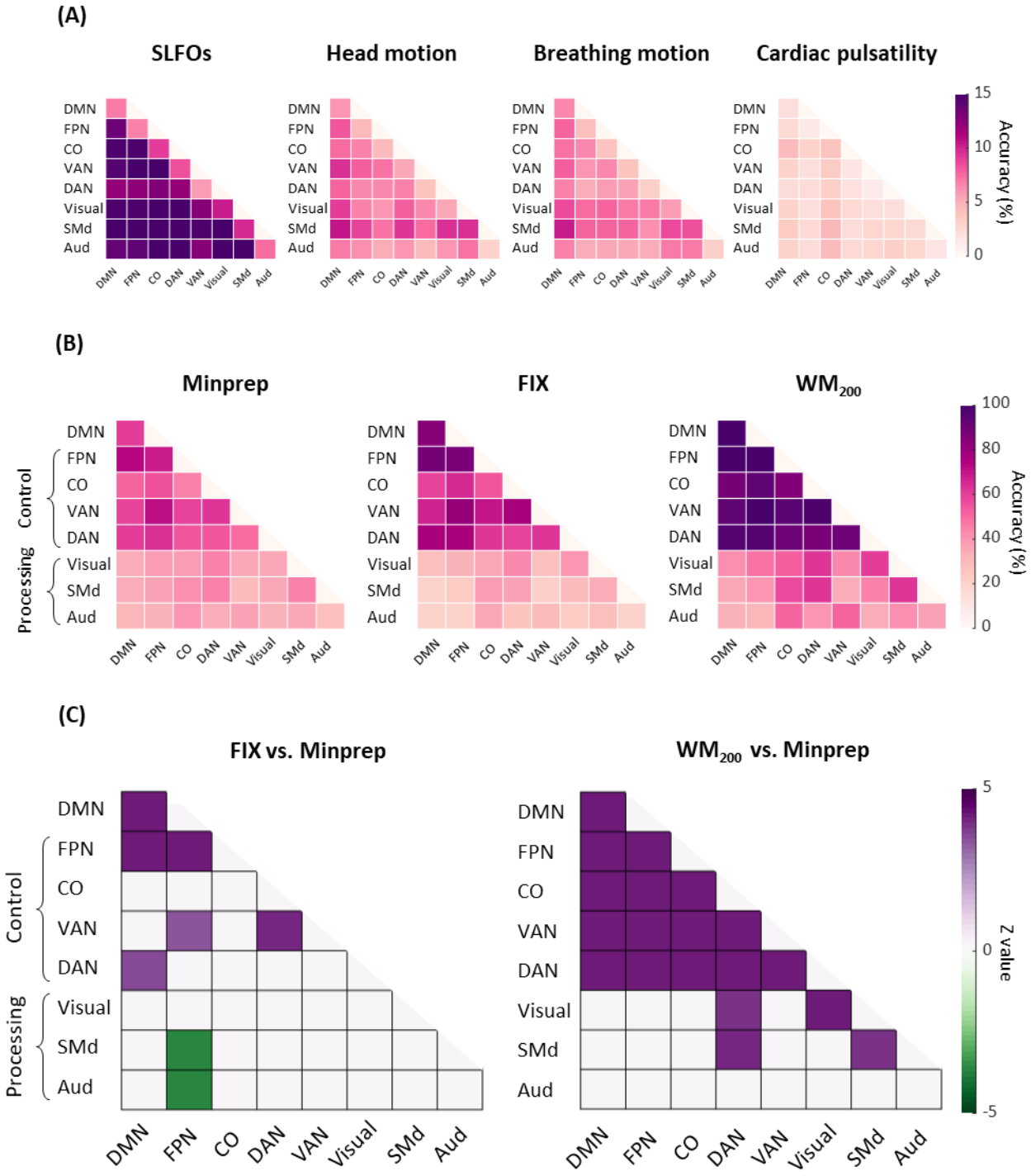

Figure 6. Connectome fingerprinting results using edges from within and between networks. (A) Fingerprinting accuracy for SLFOs, head motion, breathing motion and cardiac pulsatility, averaged across all database-target pairs. **(B)** Fingerprinting accuracy for Minprep, FIX and WM_{200} pipelines, averaged across all database-target pairs. **(C)** Significant differences in fingerprinting accuracy for FIX and WM_{200} pipelines compared to the Minprep pipeline ($p<0.05$, Bonferroni corrected, Wilcoxon ranksum).

3.5 Capability of preprocessing strategies to remove the nuisance signatures on time-varying FC at the individual level

To examine the effect of physiological processes and head motion on time-varying FC estimates, we computed functional connectivity dynamics (FCD) matrices (Hansen *et al.*, 2015) using the generated nuisance and "neural" datasets from each scan, where each FCD matrix captures the temporal evolution of FC patterns within a scan. We then computed the similarity of the nuisance and "neural" FCD matrices at the individual level to examine the capability of various preprocessing strategies to reduce the bias introduced by physiological processes and head motion on time-varying FC. A distribution of the similarity values, in this case Pearson's correlation coefficients, is shown in **Figure 7** for each preprocessing strategy and nuisance process. We observed that the temporal evolution of FC patterns from SLFOs and head motion were similar to the ones observed in the Minprep data. An illustration of this association is shown in **Figure 8** for six subjects. On the other hand, breathing motion and cardiac pulsatility FCD matrices did not seem to resemble the FCD matrices from "neural" datasets (**Figure 7**).

The signature induced by SLFOs on time-varying FC remained after all preprocessing pipelines were applied, but was considerably reduced by the WM_{50} and WM_{200} strategies (**Figure 7A**, **Figure 8**). FIX denoising was the least successful strategy to reduce the SLFOs signature (**Figure 7A**, **Figure 8**), as in static FC (**Figure 4E**), and only achieved the same level of correction as other strategies after GSR. However, even after GSR none of the strategies reached chance levels (**Figure 7A**), in contrast with the static FC results (**Figure 4E**). The signature related to head motion was not entirely eradicated by any of the approaches examined, but was considerably reduced by the WM_{50} and WM_{200} strategies (**Figure 7B**). GSR slightly reduced the similarity between the head motion and "neural" FCD matrices (**Figure 7B**), as in static FC (**Figure 4F**).

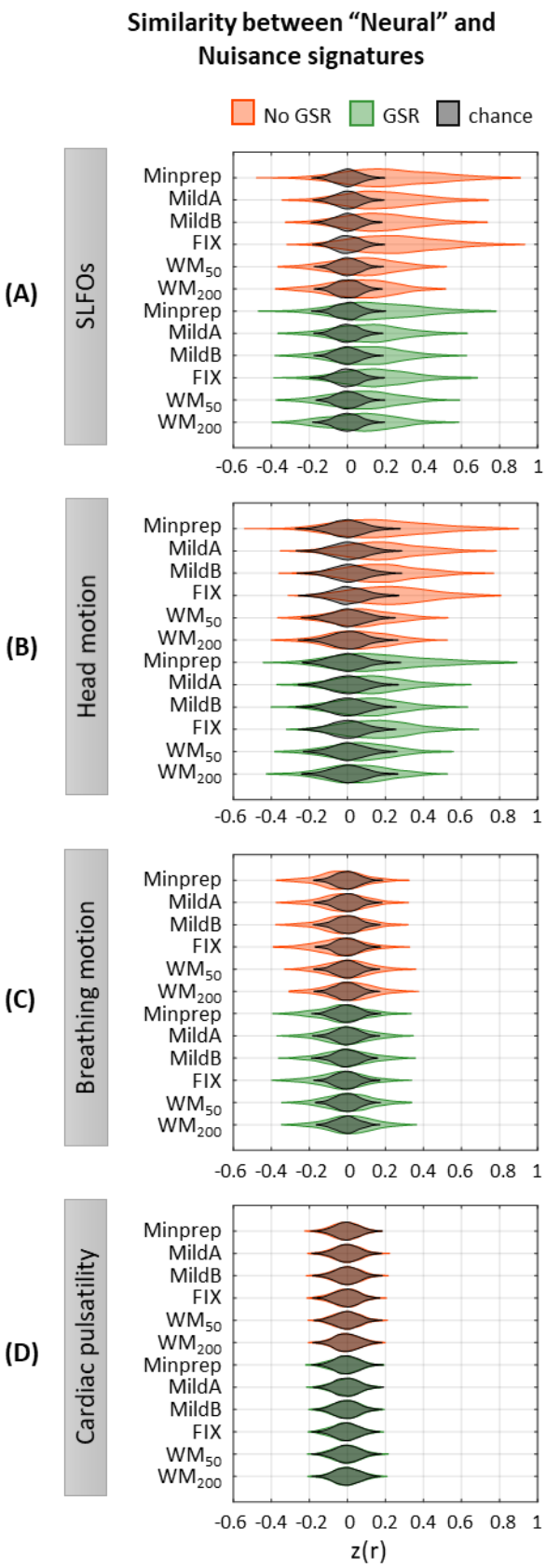

Figure 7. Time-varying FC.

Distribution of Pearson correlation coefficients across all 1,568 scans between the "neural" functional connectivity dynamics (FCD) matrix after each preprocessing pipeline and nuisance FCD matrices associated to **(A)** SLFOs, **(B)** head motion, **(C)** breathing motion, and **(D)** cardiac pulsatility. Correlation values were Fisher z transformed. Note that correlation coefficients identified as outliers (> 3 SD) were disregarded.

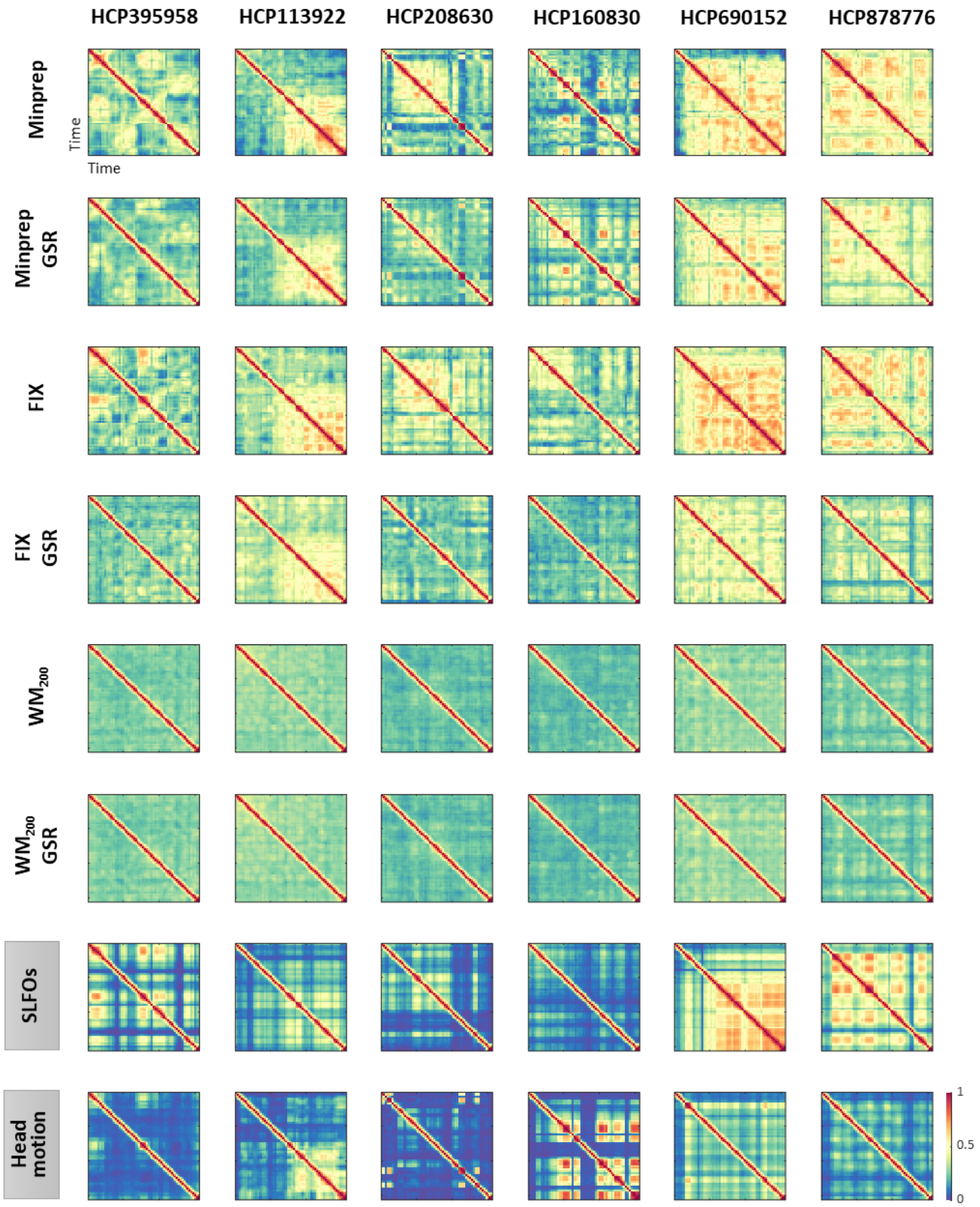

Figure 8. Time-varying FC. Illustrative examples of FCD matrices from specific HCP subjects for several pre-processing pipelines (rows 1-6) and SLFOs and head motion (rows 7 and 8, respectively). All the examples are from the HCP scan Rest1_LR. These examples showcase a large resemblance between FCD matrices computed from the "neural" datasets and the nuisance datasets of SLFOs and head motion.

4 Discussion

In this work, we set out to characterize physiological and head motion biases on static and time-varying FC measures, as well as to investigate the implications of these biases for connectome fingerprinting analyses. Utilizing physiological recordings and resting-state fMRI data from the HCP dataset, we found that physiological processes and head motion exert a stereotyped influence on static FC (**Figure 4A-D**), and that recurring patterns in time-varying FC can be attributed, to some extent, to SLFOs and head motion (**Figure 7**, **Figure 8**). Aggressive preprocessing strategies such as FIX (Salimi-Khorshidi *et al.*, 2014) and WM denoising (Kassinopoulos and Mitsis, 2019b) combined with GSR were the most effective to decrease the physiological and head motion signatures on FC, albeit none of the strategies completely removed all the sources of noise (**Figure 4E-H**, **Figure 7**, **Figure 8**). In this work, we also performed connectome fingerprinting by utilizing the four resting-state scans of each subject. Our results demonstrated that removal of nuisance processes increases identification accuracy in connectome fingerprinting (**Figure 5B**). This observation indicates that subject-specific artifacts are not the main basis behind individual discriminability, which suggests a neural origin underpinning the inter-individual differences in connectivity.

4.1 Spatially heterogeneous contributions of nuisance processes on the BOLD signal

It is well established that head and breathing motion affect areas at the edges of the brain, whereas cardiac pulsatility affects areas around the brainstem. However, as these maps are typically reported in the volumetric space, we cannot easily appreciate whether fluctuations in atlas-based ROIs have contributions from these nuisance processes. In principle, it could be the case that artifacts associated with a specific nuisance process demonstrate significant variability in their waveform across voxels, and as a result their effects cancel out when averaging voxels within an ROI. In this study, we assessed the impact and regional variation of these nuisance processes in the Gordon atlas, a widely used atlas in the literature.

SLFOs related to changes in heart rate and breathing patterns were found to affect mostly sensory regions including visual cortex and somatosensory cortex (particularly of the face) (**Figure 3A**), which correspond to regions with high density of veins, for instance the straight and the transverse sinuses. The spatial pattern of SLFOs is very similar to statistical maps reported in prior work showing brain regions highly correlated with the global signal (Tong *et al.*, 2013; Glasser *et al.*, 2016; Power *et al.*, 2017; Li, Bolt, *et al.*, 2019; Zhang *et al.*, 2019). This is not surprising, since the global signal is strongly driven by fluctuations in heart rate and breathing patterns (Birn *et al.*, 2006; Shmueli *et al.*, 2007; Chang and Glover, 2009a; Falahpour, Refai and Bodurka, 2013; Kassinopoulos and Mitsis, 2019a). Moreover, we show evidence that SLFOs and cardiac pulsatility do not affect the same brain regions, consistent with (Tong and Frederick, 2014; Chen, Polimeni, *et al.*, 2019; Kassinopoulos and Mitsis, 2019a).

Specifically, cardiac pulsatility was more dominant in regions such as the insular and auditory cortices, which aligns with cortical branches of the middle cerebral artery (**Figure 3D**) and are the regions with highest arterial density (Bernier, Cunnane and Whittingstall, 2018).

Regarding head motion, previous studies found that its effect was more pronounced in prefrontal, sensorimotor and visual brain regions (Satterthwaite *et al.*, 2013; Yan *et al.*, 2013). However, these studies did not remove breathing artifacts from the realignment parameters, which are present even in single-band datasets (Gratton, Coalson, *et al.*, 2019), and thus were unable to disentangle whether a specific type of motion affected particular brain regions. In this work we regressed out breathing motion from the realignment parameters, and observed that sensorimotor and visual areas were strongly affected by head motion (**Figure 3B**), whereas breathing motion artifacts were more pronounced in prefrontal cortex and brain regions in parietal and temporal cortices (**Figure 3C**). Furthermore, Yan et al. showed that framewise displacement was positively correlated with sensory regions and negatively correlated with prefrontal regions. Collectively, these findings suggest that most regions exhibit an increase in the BOLD signal due to head and breathing motion, whereas prefrontal cortex may exhibit a decrease in the BOLD signal likely due to breathing-related chest movements.

4.2 Physiological and head motion signatures in static FC

Head motion is considered the biggest concern for FC fMRI studies and there is a significant effort from the neuroimaging field on developing and evaluating preprocessing strategies that mitigate its associated effects (Power, Schlaggar and Petersen, 2015; Ciric *et al.*, 2017; Parkes *et al.*, 2018). On the other hand, while it has been shown that SLFOs affect the default-mode network (Birn, Murphy and Bandettini, 2008; Chang and Glover, 2009a; Birn *et al.*, 2014), and high frequency cardiac and breathing artifacts influence the BOLD signal (Glover, Li and Ress, 2000; Power *et al.*, 2019), the effects of physiological processes have not yet been examined for whole-brain FC. In this study we evaluated collectively the impact of the aforementioned sources of noise in fMRI in the context of whole-brain FC at rest.

Our results revealed that all four nuisance datasets exhibited mainly positive correlations between ROIs (**Figure 4A-D**), suggesting that the presence of nuisance fluctuations in a conventional fMRI dataset typically leads to a shift of correlation values towards positive numbers. In other words, in the case of an fMRI dataset that has not been corrected for nuisance fluctuations, two ROIs whose neural-related fluctuations are negatively correlated could be found to be unrelated or even positively correlated due to the presence of similar nuisance fluctuations in the ROIs. Furthermore, we observed that SLFOs and head motion confounded FC to a larger degree compared to breathing motion and cardiac pulsatility (**Figure 4E-H**).

Our results suggest that SLFOs due to spontaneous changes in heart rate or breathing patterns inflate connectivity (toward positive values) across the whole brain but particularly edges within the visual networks as well as edges between the visual and the rest of the networks (**Figure 4A**). It is well known that the visual cortex presents the highest venous density (Bernier, Cunnane and Whittingstall, 2018), possibly due to its functional importance (Collins *et al.*, 2010). In addition, it has been shown that brain regions with higher vascular density exhibit larger amplitude of spontaneous BOLD fluctuations (Vigneau-Roy *et al.*, 2014). As such, we believe that the structure of the SLFOs' FC signature may be the result of the vascular architecture. The effect of SLFOs on static FC was considerably reduced after WM denoising, and after GSR it almost vanished (Fig. 4E). Notably, FIX denoising without GSR was unable to remove the bias introduced by SLFOs, which is consistent with recent studies showing that global artifactual fluctuations are still prominent after FIX denoising (Burgess *et al.*, 2016; Power *et al.*, 2017, 2018; Glasser *et al.*, 2018; Kassinopoulos and Mitsis, 2019a).

Head motion was found to influence the connectivity within visual and sensorimotor networks (**Figure 4B**), in line with previous studies (Power *et al.*, 2012; Satterthwaite *et al.*, 2012; van Dijk, Sabuncu and Buckner, 2012). Our results showed that only regressing out the realignment parameters and average WM/CSF signals (with or without expansion terms) is not sufficient to remove the effects of head motion (**Figure 4F**, MildA and MildB pipelines), which is consistent with findings in (Parkes *et al.*, 2018). Among all preprocessing strategies, WM denoising yielded the largest reduction in motion biases (**Figure 4F**). The two pipelines WM_{50} and WM_{200} refer to the removal of 50 and 200 white matter regressors from the data (i.e. principal components obtained from the white matter compartment). In our previous study we showed that while both pipelines exhibit high large-scale identifiability compared to other pipelines, the aggressive pipeline WM_{200} shows stronger reduction in motion artifacts and biases compared to WM_{50} (Kassinopoulos and Mitsis, 2019b). Although not as clear as in the previous study, our results show a stronger reduction of head motion effects for the former compared to the latter (**Figure 4F**). This result may explain also the higher accuracy in connectome fingerprinting observed for the pipeline WM_{200} compared to the WM_{50}.

A natural concern regarding the head motion signature would be the possibility that it reflects motor-related activity (Yan *et al.*, 2013). Note that the head motion signature was derived from the motion traces estimated during volume realignment. Even though motor-related neural activity would be expected to lag the instantaneous motion traces due to the sluggishness of the hemodynamic response, we cannot exclude the scenario that the head motion signature reflects motor-related neural activity. Nonetheless, we believe that even if preprocessing strategies remove neural activity associated with spontaneous head movements, this source of neural activity is typically of no interest in resting-state fMRI studies.

Furthermore, we provide evidence that head and breathing motion do not bias functional connectivity in the same way. Specifically, breathing motion was found to inflate within-hemisphere connectivity (**Figure 4C**). This bias

seems to arise as a result of factitious motion rather than real motion of the head, since it is related to the LR/RL phase encoding direction (see section 4.4 for more details). All preprocessing strategies yielded a substantial reduction in biases related to breathing motion, with FIX denoising being the most effective (**Figure 4G**).

In our dataset, cardiac pulsatility did not seem to have a large effect on FC, neither in cortical nor subcortical regions (**Figure 4D**, **Supp. Fig. 8D**), and its effect was entirely removed with aggressive pipelines such as FIX and WM denoising (**Figure 4H**), as well as with model-based techniques (**Supp. Fig. 6D**). However, it has been recently shown that the 3T HCP dataset has poor temporal signal-to-noise ratio in the subcortex (Ji *et al.*, 2018; Seitzman, Gratton, Marek, *et al.*, 2019). Therefore, it is possible that we might have underestimated the effect of cardiac pulsatility in functional connections involving subcortical regions.

It is important to note that our proposed methodology assumes that the stereotyped nuisance signatures in FC do not resemble the true neural signatures. However, in principle, nuisance fluctuations could give rise to similar spatial patterns as neurally-driven fluctuations. A recent study by (Bright *et al.*, 2018) provided evidence that physiological fluctuations (end-tidal CO_2) give rise to networks that spatially resemble neurally-driven networks linked to working memory and visual stimuli. The authors suggested that this phenomenon may be due to the vasculature adapting to the neural network architecture, as vascular and neuronal growth processes evolve concurrently during development (Quaegebeur, Lange and Carmeliet, 2011). These findings suggest a caveat of our methodology when assessing pre-processing strategies, as pipelines that yield the lowest similarity between nuisance and "neural" FC matrices might also remove signal of interest. Nonetheless, the pre-processing strategies that were found in this study to reduce the nuisance effects the most (i.e. FIX and WM denoising combined with GSR) have been shown in an earlier study to demonstrate the highest improvement in large-scale network identifiability (Kassinopoulos and Mitsis, 2019b). In addition, these pipelines were found to exhibit the highest accuracy in connectome fingerprinting (**Figure 5B**). Therefore, these pipelines seem to remove adequately the effects of nuisance processes while also preserving the signal of interest.

Importantly, even with aggressive preprocessing approaches, residual relationships between nuisance processes and FC measures remain a concern when investigating interindividual and/or group differences (Ciric *et al.*, 2017; Parkes *et al.*, 2018; Nalci, Luo and Liu, 2019). Several researchers have recommended to covary motion effects at the group-level (Satterthwaite et al. 2012, Fair et al. 2012). Since SLFOs refer to fluctuations in heart rate and breathing pattern, we believe that it would be a good practice to also covary physiological metrics such as the variance in heart rate and breathing rate at the group-level.

4.3 Physiological and head motion signatures in time-varying FC

The investigation of neural dynamics through resting-state fMRI is a promising avenue of research that has gained increasing attention lately (Hutchison *et al.*, 2013; Lurie *et al.*, 2019). Yet, there is skepticism regarding its validity and underlying origins. For instance, variations in FC over shorter time-scales (i.e. minutes) could largely be explained by sampling error, acquisition artifacts and subject arousal (Laumann *et al.*, 2017).

In this study, we computed time-resolved FC dynamics (Hansen *et al.*, 2015) in both nuisance and "neural" datasets to evaluate whether non-neural fluctuations could partly explain the recurrent connectivity patterns observed in fMRI studies. The FC dynamics of head motion and SLFOs datasets were markedly similar to the FC dynamics observed in "neural" datasets (**Figure 7A-B**), albeit the similarity was smaller than for static FC (**Figure 4E-F**). Looking at the time-resolved FC matrices (**Figure 8**) is quite apparent that a large component of variability in FC patterns is due to non-neural processes, and that these patterns remain after widely used pipelines such as MildA, MildB and FIX. These results are aligned with the observation that even after regressing out nuisance processes from BOLD signals, correlations between time-varying FC measures and nuisance fluctuations remain (Nalci, Rao and Liu, 2019). WM denoising was the best strategy to mitigate the influence of nuisance processes (**Figure 7A-B**).

After WM denoising, variability in FC patterns was greatly diminished (**Figure 8**), even when those patterns could not be directly associated with any nuisance process (**Supp. Fig. 7**). These results can be interpreted in two ways that are not mutually exclusive: (1) Most observations of variability in FC patterns are a result of non-neural confounds and WM denoising is able to remove a significant fraction of these confounds. This is supported by the fact that many other nuisance processes can influence the BOLD signal that we did not examine here (e.g. arterial blood pressure, CO_2 concentration, scanner instabilities). (2) WM denoising removes variance of neural origin. Future work with concurrent direct measurements of neuronal activity (e.g. electroencephalography, calcium imaging) and physiological recordings may prove instrumental to resolve to which extent time-varying FC is the result of underlying neural dynamics.

While head motion and SLFOs were found to be strongly associated to recurrent connectivity patterns, breathing motion and cardiac pulsatility did not seem to be a main concern for time-varying FC studies (**Figure 7C-D**). Likely, the effects of breathing motion and cardiac pulsatility do not influence time-varying FC because their effect on the BOLD signal does not change from window to window due to their quasi-periodic nature. In contrast, the levels of head motion vary across time windows. Similarly, heart rate and breathing patterns can be quite constant for some time periods, in which case SLFOs do not influence the BOLD signal and in turn FC, whereas for other time periods heart rate and breathing patterns change considerably, in which case SLFOs influence the BOLD signal and leave their imprint in time-varying FC. In other words, ROIs sensitive to head motion and SLFOs exhibit a time-varying

signal-to-noise ratio depending on the presence of these sources of noise, which leads to confounds in the time-varying FC measures.

Importantly, none of the evaluated pipelines was able to completely remove these confounds. It was only recently that researchers have started to examine the performance of pre-processing pipelines in the context of time-varying FC (Lydon-Staley *et al.*, 2019), albeit with a focus on motion effects, thus more work is needed to identify effective data cleaning strategies for resting-state time-varying FC studies.

4.4 Global signal regression

The practise of removing the GS from fMRI data (i.e. GSR) has been adopted by many fMRI investigators as the global signal has been linked to head motion artifacts and fluctuations in heart rate and breathing patterns (Birn *et al.*, 2006; Shmueli *et al.*, 2007; Chang and Glover, 2009a; Falahpour, Refai and Bodurka, 2013; Power *et al.*, 2014, 2018; Byrge and Kennedy, 2018; Kassinopoulos and Mitsis, 2019a). Further, GSR has been shown to increase the resemblance of FC correlations to electrophysiological measures (Keller *et al.*, 2013) and strengthen the association between FC and behaviour (Li, Kong, *et al.*, 2019). On the other hand, studies capitalizing on EEG-fMRI data have reported an association between the GS amplitude and vigilance measures (Wong *et al.*, 2013, 2016) and individual differences in the global signal topography have been related to behavior and cognition (Li, Bolt, *et al.*, 2019). Thus, as it is not clear whether it removes neuronal-related activity, GSR still remains a controversial pre-processing step (Liu, Nalci and Falahpour, 2017; Murphy and Fox, 2017).

Our results provide evidence that, in static FC, GSR removes physiological fluctuations related to SLFOs and to a lesser extent head motion artifacts (**Figure 4E-F**). Note that GSR does not account for breathing motion artifacts (**Figure 4G**) rather than changes in breathing patterns and deep breaths, which are related to SLFOs and perhaps the head motion component at ~0.12 Hz (Power *et al.*, 2019). Furthermore, GSR improved connectome fingerprinting accuracy (**Figure 5B**), which suggests that by removing nuisance fluctuations due to SLFOs and head motion, GSR enhances the individual connectivity profiles. Overall, our results suggest that GSR leads to such a strong reduction in the effects of SLFOs and head motion that even if a small fraction of neuronal-driven fluctuations is lost, the ultimate quality of the cleaned data is overall improved. GSR is particularly important when using ICA-based noise correction techniques such as FIX and AROMA (Salimi-Khorshidi *et al.*, 2014; Pruim *et al.*, 2015), since ICA components related to SLFOs have similar spatial pattern and frequency profile as neural components and thus are not classified as artifacts.

Regarding time-varying FC, GSR did not reduce the effect of nuisance processes as well as in the static FC scenario (**Figure 4E-F** vs. **Figure 7A-B**). Nonetheless, a recent study evaluating preprocessing strategies in the context of time-varying FC showed that incorporating GSR in the preprocessing improved the identification of modularity in

functional networks (Lydon-Staley *et al.*, 2019). This may indicate that GSR was able to remove nuisance processes that we did not evaluate in the current study. These processes may be related to scanner instabilities, CO_2 concentration (Wise *et al.*, 2004; Power *et al.*, 2017) and finger skin vascular tone (Özbay *et al.*, 2019) that are known to be reflected on the GS.

Despite the effectiveness of GSR in reducing nuisance confounds from the data, we cannot exclude the possibility of removing some neuronal-related fluctuations. Alternatives to GSR that have been proposed to remove global artifacts include time delay analysis using "rapidtide" (Tong, Hocke and Frederick, 2019), removal of the first principal component from the data (Carbonell, Bellec and Shmuel, 2011), removal of fluctuations associated to large clusters of coherent voxels (Aquino *et al.*, 2019), and the use of temporal ICA (Glasser *et al.*, 2018), albeit the latter is only applicable to large datasets such as HCP.

4.5 The effect of phase encoding direction in connectivity

Early studies demonstrated that chest wall movements due to breathing perturb the B_0 field (Raj *et al.*, 2000; Raj, Anderson and Gore, 2001; Van de Moortele *et al.*, 2002), which has consequences in EPI fMRI data. While this phenomenon is not fully understood, it seems to have two main effects that are observable along the phase encoding direction: (1) Breathing causes factitious motion of the fMRI volumes in the phase encoding direction (Raj *et al.*, 2000; Raj, Anderson and Gore, 2001), which has sparkled attention recently since it has been recognised that this effect has critical implications for motion correction when performing censoring (i.e. removal of motion-contaminated fMRI volumes) in multi-band (Fair *et al.*, 2019; Power *et al.*, 2019) and single-band (Gratton, Coalson, *et al.*, 2019) data. (2) Breathing induces artifacts on voxel timeseries that depend on the location of those voxels along the phase encoding direction (Raj *et al.*, 2000; Raj, Anderson and Gore, 2001). Our results provide further evidence for the latter. Specifically, we found that depending on whether the phase encoding direction was LR or RL, breathing motion artifacts were more pronounced on the left or right hemisphere, respectively (**Figure 3C**). Moreover, we observed that breathing motion increased within-hemisphere connectivity for both phase encoding scans (**Figure 4C**, **Supp. Fig. 4C**), which implies that breathing induces artifactual fluctuations that are to a certain extent different between hemispheres. Note though that the signature of breathing motion exhibited some differences for the two phase encoding directions (**Supp. Fig. 4C**), which explains the higher connectome fingerprinting accuracy in the breathing motion dataset when examining pairs of scans with same phase encoding direction compared to scans with different phase encoding direction (**Figure 5A**).

Our results point to a systematic effect of breathing on static FC through variations in the B_0 magnetic field. Importantly, this systematic bias is contingent on the phase encoding direction which seems to indicate that factitious rather than real motion is the predominant source of respiration-related motion artifacts in fMRI, as has been previously suggested (Raj, Anderson and Gore, 2001; Brosch *et al.*, 2002). Even though common

preprocessing pipelines greatly reduce these effects, they do not eliminate them (**Figure 4C**). Thus, studies that consider datasets with different phase encodings, should be aware of the effect of phase encoding on FC, especially if different groups have been acquired with different phase encodings.

4.6 Individual discriminability

Test-retest reliability is important for establishing the stability of inter-individual variation in fMRI FC. However, apart from neural processes, nuisance processes can also have an impact on test-retest reliability, given the high subject-specificity of physiological processes and head motion. This leads to the concerning notion that nuisance processes may be artifactually driving the reports of high reliability in FC measures. Some indications that confounds might be artifactually increasing test-retest reliability are the following ones: the median of intraclass correlation values across functional connections, which is a metric of test-retest reliability, is reduced when a relatively aggressive pipeline is used (Birn *et al.*, 2014; Parkes *et al.*, 2018), motion can classify subjects at above-chance levels (Horien *et al.*, 2019), and breathing motion related to phase encoding is more prominent in older individuals and those with a higher body mass index (Gratton, Coalson, *et al.*, 2019). In this study, we examined the potential effect of nuisance processes on subject discriminability in the context of connectome fingerprinting.

4.6.1 Whole-brain identification

To address the individual discriminability of nuisance processes, we performed connectome fingerprinting analysis using the generated nuisance datasets. All nuisance processes exhibited identification accuracy higher than chance (**Figure 5A**). Pairs of scans with the same phase encoding showed higher identification accuracy than pairs of scans with different phase encoding (**Figure 5A**). This effect is particularly evident for breathing motion, and to a lesser extent for cardiac pulsatility and head motion. This observation suggests that not only these confounds exert a distinctive artifactual spatial pattern that is dependent on the phase encoding direction, which could be speculated based on careful examination of **Figure 3B-D**, but also that this artifactual pattern is to a certain degree specific to the individual. Likely, this is as a result of individual differences in brain anatomy. On the other hand, the subject discriminability for SLFOs is not modulated by phase encoding (**Figure 5A**). Given the nature of SLFOs (i.e. it affects the BOLD signal through changes in CBF), the high subject discriminability of SLFOs suggests a certain degree of idiosyncrasy that is possibly related to the vascular architecture of an individual. Overall, our results suggest that there is some degree of subject discriminability in nuisance processes.

Identification accuracies of "neural" datasets were very high for all preprocessing strategies (**Figure 5B**), in line with previous studies (Finn *et al.*, 2015; Horien *et al.*, 2019). WM denoising, which was the most effective strategy in reducing confounds due to head motion and physiological fluctuations (**Figure 4E-H**), yielded also the highest

accuracy in connectome fingerprinting (**Figure 5B**), suggesting that the high subject discriminability observed in the HCP data is not due to the presence of confounds. Interestingly, the increased accuracy observed in the nuisance datasets for scans with the same phase encoding (**Figure 5A**) is also observed in the Minprep data (**Figure 5B**). In contrast, for the rest of the pipelines the difference in accuracy between pairs of scans from different days with the same or different phase encoding direction vanishes (**Figure 5B**). This is likely because of the reduction of nuisance effects, mainly breathing motion artifacts. Note also that for both mild and aggressive pipelines, pairs of scans from the same day exhibited higher accuracies compared to pairs of scans from different days which cannot be attributed to potential residuals of nuisance fluctuations (**Figure 5A**). Possible explanations for this finding is that the functional connectome of a subject reflects some aspects of their vigilance levels (Thompson, Magnuson, *et al.*, 2013; Tagliazucchi and Laufs, 2014; Wang *et al.*, 2016), mind-wandering (Gorgolewski *et al.*, 2014; Kucyi and Davis, 2014; Kucyi, 2018; Gonzalez-Castillo *et al.*, 2019), or the effect of time of day (Shannon *et al.*, 2013; Hodkinson *et al.*, 2014; Jiang *et al.*, 2016; Orban *et al.*, 2019), which can differ across sessions. Overall, the high connectome-based identification accuracies reported in the literature do not appear to be driven by nuisance confounds, suggesting a neural origin underpinning the inter-individual differences in connectivity.

4.6.2 Network-based identification

We found that that individuals demonstrate distinct FC relative to the group most frequently in association cortices (e.g., parts of the frontoparietal, default mode, and cinguloopercular systems) (**Figure 6B**), consistent with previous studies (Mueller *et al.*, 2013; Finn *et al.*, 2015; Vanderwal *et al.*, 2017; Gratton *et al.*, 2018; Horien *et al.*, 2019; Seitzman, Gratton, Laumann, *et al.*, 2019). The fact that association cortices are the most evolutionarily recent (Zilles *et al.*, 1988) and are thought to be involved in higher-level functions (Dosenbach *et al.*, 2007; Cole *et al.*, 2013; Cole, Repovš and Anticevic, 2014; Raichle, 2015; Gratton *et al.*, 2017) has been posited as a possible reason for the high identification accuracy of these networks. On the other hand, it has also been speculated that medial frontal and frontoparietal networks exhibit the highest identification accuracy as a result of being less prone to distortions from susceptibility artifacts (Noble *et al.*, 2017; Horien *et al.*, 2019). If the latter was the case, we would expect to see decreased accuracy for these networks when probing the nuisance datasets. However, we did not observe such a tendency for any of the nuisance processes evaluated (**Figure 6A**), and preprocessing strategies that successfully removed nuisance processes showed enhanced subject discriminability of control networks and DMN (**Figure 6C**). These results seem to indicate that the basis of the high identification rates for association cortices is of neural origin, and thus that resting-state fMRI-based connectome fingerprinting can capture idiosyncratic aspects of cognition underlain by the association cortex.

5 Conclusions

The current study introduces a new framework for assessing potential signatures (systematic biases) of physiological processes and head motion on static and time-varying FC. SLFOs associated to changes in heart rate and breathing patterns as well as head motion exhibited the strongest biases in both static and time-varying FC. Aggressive preprocessing strategies (i.e. FIX and WM denoising) in conjunction with GSR lead to the strongest mitigation of physiological and head motion signatures. These pipelines demonstrated the highest identification accuracy suggesting that the high subject discriminability observed in connectome fingerprinting cannot be attributed to the evaluated nuisance confounds.

Acknowledgments

This work was supported by the Natural Sciences and Engineering Research Council of Canada (Discovery Grant 34362 awarded to GDM), the Fonds de la Recherche du Quebec - Nature et Technologies (FRQNT; Team Grant PR191780-2016 awarded to GDM) and the Canada First Research Excellence Fund (awarded to McGill University for the Healthy Brains for Healthy Lives initiative). AXP and MK acknowledge funding from Québec Bio-imaging Network (QBIN). Data were provided by the Human Connectome Project, WU-Minn Consortium (Principal Investigators: David Van Essen and Kamil Ugurbil; 1U54MH091657) funded by the 16 NIH Institutes and Centers that support the NIH Blueprint for Neuroscience Research; and by the McDonnell Center for Systems Neuroscience at Washington University. We are extremely grateful to all Human Connectome Project study participants, who generously donated their time to make this resource possible.

Competing interests

The authors declare that no competing interests exist.

Author contributions

Alba Xifra-Porxas, Conceptualization, Methodology, Software, Formal analysis, Investigation, Data curation, Visualization, Writing–original draft, Writing–review & editing

Michalis Kassinopoulos, Conceptualization, Methodology, Investigation, Data curation, Writing–review & editing

Georgios D. Mitsis, Conceptualization, Supervision, Writing–review & editing

References

Aquino, K. M. *et al.* (2019) 'Identifying and removing widespread signal deflections from fMRI data: Rethinking the global signal regression problem', *bioRxiv*, p. 662726. doi: 10.1101/662726.

Baker, A. P. *et al.* (2014) 'Fast transient networks in spontaneous human brain activity', *eLife*, 2014(3), pp. 1–18. doi: 10.7554/eLife.01867.

Baker, J. T. *et al.* (2014) 'Disruption of cortical association networks in schizophrenia and psychotic bipolar disorder', *JAMA Psychiatry*, 71(2), pp. 109–118. doi: 10.1001/jamapsychiatry.2013.3469.

Batchvarov, V. N. *et al.* (2002) 'QT-RR relationship in healthy subjects exhibits substantial intersubject variability and high intrasubject stability', *American Journal of Physiology - Heart and Circulatory Physiology*, 282(6 51-6), pp. 2356–2363. doi: 10.1152/ajpheart.00860.2001.

Battaglia, D. *et al.* (2017) 'Functional Connectivity Dynamics of the Resting State across the Human Adult Lifespan', *bioRxiv*, p. 107243. doi: 10.1101/107243.

Bernier, M., Cunnane, S. C. and Whittingstall, K. (2018) 'The morphology of the human cerebrovascular system', *Human Brain Mapping*, (March), pp. 1–14. doi: 10.1002/hbm.24337.

Birn, R. M. *et al.* (2006) 'Separating respiratory-variation-related fluctuations from neuronal-activity-related fluctuations in fMRI', *NeuroImage*, 31(4), pp. 1536–1548. doi: 10.1016/j.neuroimage.2006.02.048.

Birn, R. M. *et al.* (2008) 'The respiration response function: The temporal dynamics of fMRI signal fluctuations related to changes in respiration', *NeuroImage*. Elsevier Inc., 40(2), pp. 644–654. doi: 10.1016/j.neuroimage.2007.11.059.

Birn, R. M. *et al.* (2014) 'The influence of physiological noise correction on test-retest reliability of resting-state functional connectivity', *Brain connectivity*, 4(7), pp. 511–522. doi: 10.1089/brain.2014.0284.

Birn, R. M., Murphy, K. and Bandettini, P. A. (2008) 'The effect of respiration variations on independent component analysis results of resting state functional connectivity', *Human Brain Mapping*, 29(7), pp. 740–750. doi: 10.1002/hbm.20577.

Biswal, B. *et al.* (1995) 'Functional connectivity in the motor cortex of resting human brain using echo-planar MRI', *Magnetic Resonance in Medicine*. doi: 10.1002/mrm.1910340409.

Bright, M. G. *et al.* (2018) 'Vascular physiology drives functional brain networks', *bioRxiv*, p. 475491. doi: 10.1101/475491.

Bright, M. G. and Murphy, K. (2015) 'Is fMRI "noise" really noise? Resting state nuisance regressors remove variance with network structure', *NeuroImage*. Elsevier B.V., 114, pp. 158–169. doi: 10.1016/j.neuroimage.2015.03.070.

Bright, M. G., Tench, C. R. and Murphy, K. (2017) 'Potential pitfalls when denoising resting state fMRI data using nuisance regression', *NeuroImage*. Elsevier, 154(December 2016), pp. 159–168. doi: 10.1016/j.neuroimage.2016.12.027.

Brookes, M. J. *et al.* (2011) 'Measuring functional connectivity using MEG: Methodology and comparison with fcMRI', *NeuroImage*. Elsevier Inc., 56(3), pp. 1082–1104. doi: 10.1016/j.neuroimage.2011.02.054.

Brosch, J. R. *et al.* (2002) 'Simulation of human respiration in fMRI with a mechanical model', *IEEE Transactions on Biomedical Engineering*. IEEE, 49(7), pp. 700–707. doi: 10.1109/TBME.2002.1010854.

Burgess, G. C. *et al.* (2016) 'Evaluation of Denoising Strategies to Address Motion-Correlated Artifacts in Resting-State Functional Magnetic Resonance Imaging Data from the Human Connectome Project', *Brain Connectivity*, 6(9), pp. 669–680.

doi: 10.1089/brain.2016.0435.

Byrge, L. and Kennedy, D. P. (2018) 'Identifying and characterizing systematic temporally-lagged BOLD artifacts', *NeuroImage*. Elsevier Ltd, 171(December 2017), pp. 376–392. doi: 10.1016/j.neuroimage.2017.12.082.

Caballero-Gaudes, C. and Reynolds, R. C. (2017) 'Methods for cleaning the BOLD fMRI signal', *NeuroImage*. Elsevier, 154(December 2016), pp. 128–149. doi: 10.1016/j.neuroimage.2016.12.018.

Carbonell, F., Bellec, P. and Shmuel, A. (2011) 'Global and System-Specific Resting-State fMRI Fluctuations Are Uncorrelated: Principal Component Analysis Reveals Anti-Correlated Networks', *Brain Connectivity*, 1(6), pp. 496–510. doi: 10.1089/brain.2011.0065.

Chan, M. Y. *et al.* (2014) 'Decreased segregation of brain systems across the healthy adult lifespan', *Proceedings of the National Academy of Sciences*, 111(46), pp. E4997–E5006. doi: 10.1073/pnas.1415122111.

Chang, C. *et al.* (2013) 'Association between heart rate variability and fluctuations in resting-state functional connectivity', *NeuroImage*. Elsevier Inc., 68, pp. 93–104. doi: 10.1016/j.neuroimage.2012.11.038.

Chang, C., Cunningham, J. P. and Glover, G. H. (2009) 'Influence of heart rate on the BOLD signal: The cardiac response function', *NeuroImage*. Elsevier Inc., 44(3), pp. 857–869. doi: 10.1016/j.neuroimage.2008.09.029.

Chang, C. and Glover, G. H. (2009a) 'Effects of model-based physiological noise correction on default mode network anti-correlations and correlations', *NeuroImage*. Elsevier Inc., 47(4), pp. 1448–1459. doi: 10.1016/j.neuroimage.2009.05.012.

Chang, C. and Glover, G. H. (2009b) 'Relationship between respiration, end-tidal CO2, and BOLD signals in resting-state fMRI', *NeuroImage*. Elsevier Inc., 47(4), pp. 1381–1393. doi: 10.1016/j.neuroimage.2009.04.048.

Chang, C. and Glover, G. H. (2010) 'Time-frequency dynamics of resting-state brain connectivity measured with fMRI', *NeuroImage*. Elsevier Inc., 50(1), pp. 81–98. doi: 10.1016/j.neuroimage.2009.12.011.

Chen, Heng *et al.* (2017) 'Intrinsic functional connectivity variance and state-specific under-connectivity in autism', *Human Brain Mapping*, 38(11), pp. 5740–5755. doi: 10.1002/hbm.23764.

Chen, J. E., Polimeni, J. R., *et al.* (2019) 'On the analysis of rapidly sampled fMRI data', *NeuroImage*. Elsevier Ltd, 188, pp. 807–820. doi: 10.1016/j.neuroimage.2019.02.008.

Chen, J. E., Lewis, L. D., *et al.* (2019) 'Resting-State "Physiological" Networks', *bioRxiv*.

Ciric, R. *et al.* (2017) 'Benchmarking of participant-level confound regression strategies for the control of motion artifact in studies of functional connectivity', *NeuroImage*, 154, pp. 174–187. doi: 10.1016/j.neuroimage.2017.03.020.

Cole, M. W. *et al.* (2013) 'Multi-task connectivity reveals flexible hubs for adaptive task control', *Nature Neuroscience*, 16(9), pp. 1348–1355. doi: 10.1038/nn.3470.

Cole, M. W., Repovš, G. and Anticevic, A. (2014) 'The frontoparietal control system: A central role in mental health', *Neuroscientist*, 20(6), pp. 652–664. doi: 10.1177/1073858414525995.

Collins, C. E. *et al.* (2010) 'Neuron densities vary across and within cortical areas in primates', *Proceedings of the National Academy of Sciences of the United States of America*, 107(36), pp. 15927–15932. doi: 10.1073/pnas.1010356107.

Dagli, M. S., Ingeholm, J. E. and Haxby, J. V. (1999) 'Localization of cardiac-induced signal change in fMRI', *NeuroImage*, 9(4), pp. 407–415. doi: 10.1006/nimg.1998.0424.

Damaraju, E. *et al.* (2014) 'Dynamic functional connectivity analysis reveals transient states of dysconnectivity in schizophrenia', *NeuroImage: Clinical*. Elsevier B.V., 5(July), pp. 298–308. doi: 10.1016/j.nicl.2014.07.003.

Demirtaş, M. *et al.* (2016) 'Dynamic functional connectivity reveals altered variability in functional connectivity among patients with major depressive disorder', *Human Brain Mapping*, 37(8), pp. 2918–2930. doi: 10.1002/hbm.23215.

van Dijk, K. R. A., Sabuncu, M. R. and Buckner, R. L. (2012) 'The influence of head motion on intrinsic functional connectivity MRI', *NeuroImage*. Elsevier Inc., 59(1), pp. 431–438. doi: 10.1016/j.neuroimage.2011.07.044.

Dosenbach, N. U. F. *et al.* (2007) 'Distinct brain networks for adaptive and stable task control in humans', *Proceedings of the National Academy of Sciences*, 104(26), pp. 11073–11078. doi: 10.1073/pnas.0704320104.

Drysdale, A. T. *et al.* (2017) 'Resting-state connectivity biomarkers define neurophysiological subtypes of depression', *Nature Medicine*. Nature Publishing Group, 23(1), pp. 28–38. doi: 10.1038/nm.4246.

Du, Y. *et al.* (2016) 'Interaction among subsystems within default mode network diminished in schizophrenia patients: A dynamic connectivity approach', *Schizophrenia Research*. Elsevier B.V., 170(1), pp. 55–65. doi: 10.1016/j.schres.2015.11.021.

Van Essen, D. C. *et al.* (2012) 'The Human Connectome Project: A data acquisition perspective', *NeuroImage*, 62(4), pp. 2222–2231. doi: 10.1016/j.neuroimage.2012.02.018.

Van Essen, D. C. *et al.* (2013) 'The WU-Minn Human Connectome Project: An overview', *NeuroImage*. Elsevier Inc., 80, pp. 62–79. doi: 10.1016/j.neuroimage.2013.05.041.

Fair, D. A. *et al.* (2019) 'Correction of respiratory artifacts in MRI head motion estimates', *NeuroImage*, p. 116400. doi: 10.1016/j.neuroimage.2019.116400.

Falahpour, M., Refai, H. and Bodurka, J. (2013) 'Subject specific BOLD fMRI respiratory and cardiac response functions obtained from global signal', *NeuroImage*. Elsevier Inc., 72, pp. 252–264. doi: 10.1016/j.neuroimage.2013.01.050.

Ferreira, L. K. *et al.* (2016) 'Aging Effects on Whole-Brain Functional Connectivity in Adults Free of Cognitive and Psychiatric Disorders', *Cerebral Cortex*, (November), pp. 3851–3865. doi: 10.1093/cercor/bhv190.

Finn, E. S. *et al.* (2015) 'Functional connectome fingerprinting: Identifying individuals using patterns of brain connectivity', *Nature Neuroscience*. Nature Publishing Group, 18(11), pp. 1664–1671. doi: 10.1038/nn.4135.

Fox, M. D. and Raichle, M. E. (2007) 'Spontaneous fluctuations in brain activity observed with functional magnetic resonance imaging', *Nat Rev Neurosci*, 8(9), pp. 700–711. doi: 10.1038/nrn2201.

Friston, K. J. *et al.* (1996) 'Movement-related effects in fMRI time-series', *Magnetic Resonance in Medicine*, 35(3), pp. 346–355. doi: 10.1002/mrm.1910350312.

Geerligs, L. *et al.* (2015) 'A Brain-Wide Study of Age-Related Changes in Functional Connectivity', *Cerebral Cortex*, 25(7), pp. 1987–1999. doi: 10.1093/cercor/bhu012.

Glasser, M. F. *et al.* (2013) 'The minimal preprocessing pipelines for the Human Connectome Project', *NeuroImage*. Elsevier Inc., 80, pp. 105–124. doi: 10.1016/j.neuroimage.2013.04.127.

Glasser, M. F. *et al.* (2016) 'The Human Connectome Project's neuroimaging approach', *Nature neuroscience*, 19(9), pp. 1175–87. doi: 10.1038/nn.4361.

Glasser, M. F. *et al.* (2018) 'Using temporal ICA to selectively remove global noise while preserving global signal in functional MRI data.', *NeuroImage*. Elsevier Inc., 181(December 2017), pp. 692–717. doi: 10.1016/j.neuroimage.2018.04.076.

Glover, G. H., Li, T. and Ress, D. (2000) 'Image-Based Method for Retrospective Correction of Physiological Motion Effects in fMRI: RETROICOR', *Magnetic Resonance in Medicine*, 44, pp. 162–167. doi: 10.1002/1522-2594(200007)44:1<162::AID-MRM23>3.0.CO;2-E.

Gonzalez-Castillo, J. *et al.* (2019) 'Imaging the spontaneous flow of thought: Distinct periods of cognition contribute to dynamic functional connectivity during rest', *NeuroImage*, 202, p. 116129. doi: 10.1016/j.neuroimage.2019.116129.

Gordon, E. M. *et al.* (2016) 'Generation and Evaluation of a Cortical Area Parcellation from Resting-State Correlations', *Cerebral Cortex*, 26(1), pp. 288–303. doi: 10.1093/cercor/bhu239.

Gorgolewski, K. J. *et al.* (2014) 'A correspondence between individual differences in the brain's intrinsic functional architecture and the content and form of self-generated thoughts', *PLoS ONE*, 9(5). doi: 10.1371/journal.pone.0097176.

Gratton, C. *et al.* (2017) 'Distinct Stages of Moment-to-Moment Processing in the Cinguloopercular and Frontoparietal Networks', *Cerebral cortex (New York, N.Y. : 1991)*, 27(3), pp. 2403–2417. doi: 10.1093/cercor/bhw092.

Gratton, C. *et al.* (2018) 'Functional Brain Networks Are Dominated by Stable Group and Individual Factors, Not Cognitive or Daily Variation', *Neuron*. Elsevier Inc., pp. 439–452. doi: 10.1016/j.neuron.2018.03.035.

Gratton, C., Koller, J. M., *et al.* (2019) 'Emergent Functional Network Effects in Parkinson Disease', *Cerebral Cortex*, 29(6), pp. 2509–2523. doi: 10.1093/cercor/bhy121.

Gratton, C., Coalson, R. S., *et al.* (2019) 'Removal of high frequency contamination from motion estimates in single-band fMRI saves data without biasing functional connectivity', *bioRxiv*. doi: 10.1101/837161.

Griffanti, L. *et al.* (2014) 'ICA-based artefact removal and accelerated fMRI acquisition for improved resting state network imaging', *NeuroImage*, 95, pp. 232–247. doi: 10.1016/j.neuroimage.2014.03.034.

Hacker, C. D. *et al.* (2017) 'Frequency-specific electrophysiologic correlates of resting state fMRI networks', *NeuroImage*. Elsevier, 149(January), pp. 446–457. doi: 10.1016/j.neuroimage.2017.01.054.

Hahamy, A., Behrmann, M. and Malach, R. (2015) 'The idiosyncratic brain: Distortion of spontaneous connectivity patterns in autism spectrum disorder', *Nature Neuroscience*, 18(2), pp. 302–309. doi: 10.1038/nn.3919.

Hallquist, M. N., Hwang, K. and Luna, B. (2013) 'The nuisance of nuisance regression: Spectral misspecification in a common approach to resting-state fMRI preprocessing reintroduces noise and obscures functional connectivity', *NeuroImage*. Elsevier Inc., 82, pp. 208–225. doi: 10.1016/j.neuroimage.2013.05.116.

Hansen, E. C. A. *et al.* (2015) 'Functional connectivity dynamics: Modeling the switching behavior of the resting state', *NeuroImage*, 105, pp. 525–535. doi: 10.1016/j.neuroimage.2014.11.001.

He, B. J. *et al.* (2008) 'Electrophysiological correlates of the brain's intrinsic large-scale functional architecture', *Proceedings of the National Academy of Sciences*, 105(41), pp. 16039–16044. doi: 10.1073/pnas.0807010105.

Hipp, J. F. *et al.* (2012) 'Large-scale cortical correlation structure of spontaneous oscillatory activity', *Nature Neuroscience*.

Hodkinson, D. J. *et al.* (2014) 'Circadian and homeostatic modulation of functional connectivity and regional cerebral blood flow in humans under normal entrained conditions', *Journal of Cerebral Blood Flow and Metabolism*, 34(9), pp. 1493–1499. doi: 10.1038/jcbfm.2014.109.

Horien, C. *et al.* (2019) 'The individual functional connectome is unique and stable over months to years', *NeuroImage*. The Authors, 189(February), pp. 676–687. doi: 10.1016/j.neuroimage.2019.02.002.

Hunyadi, B. *et al.* (2019) 'A dynamic system of brain networks revealed by fast transient EEG fluctuations and their fMRI correlates', *NeuroImage*. Elsevier Inc., 185(July 2018), pp. 72–82. doi: 10.1016/j.neuroimage.2018.09.082.

Hutchison, R. M. *et al.* (2013) 'Dynamic functional connectivity: Promise, issues, and interpretations', *NeuroImage*. Elsevier Inc., 80, pp. 360–378. doi: 10.1016/j.neuroimage.2013.05.079.

Ji, J. L. *et al.* (2018) 'Mapping the human brain's cortical-subcortical functional network organization', *NeuroImage*, 185(September 2018), pp. 35–57. doi: 10.1016/j.neuroimage.2018.10.006.

Jiang, C. *et al.* (2016) 'Diurnal variations in neural activity of healthy human brain decoded with resting-state blood oxygen level dependent fMRI', *Frontiers in Human Neuroscience*, 10(DEC2016), pp. 1–9. doi: 10.3389/fnhum.2016.00634.

Kassinopoulos, M. and Mitsis, G. D. (2019a) 'Identification of physiological response functions to correct for fluctuations in resting-state fMRI related to heart rate and respiration', *NeuroImage*. Elsevier Ltd, 202. doi: 10.1101/512855.

Kassinopoulos, M. and Mitsis, G. D. (2019b) 'White Matter Denoising Improves the Identifiability of Large-Scale Networks and Reduces the Effects of Motion in fMRI Functional Connectivity', *bioRxiv*.

Keller, C. J. *et al.* (2013) 'Neurophysiological investigation of spontaneous correlated and anticorrelated fluctuations of the BOLD signal', *Journal of Neuroscience*, 33(15), pp. 6333–6342. doi: 10.1523/JNEUROSCI.4837-12.2013.

Kucyi, A. *et al.* (2018) 'Intracranial electrophysiology reveals reproducible intrinsic functional connectivity within human brain networks', *Journal of Neuroscience*, 38(17), pp. 4230–4242. doi: 10.1523/JNEUROSCI.0217-18.2018.

Kucyi, A. (2018) 'Just a thought: How mind-wandering is represented in dynamic brain connectivity', *NeuroImage*. Elsevier Ltd, 180(July 2017), pp. 505–514. doi: 10.1016/j.neuroimage.2017.07.001.

Kucyi, A. and Davis, K. D. (2014) 'Dynamic functional connectivity of the default mode network tracks daydreaming', *NeuroImage*. Elsevier Inc., 100, pp. 471–480. doi: 10.1016/j.neuroimage.2014.06.044.

Lancaster, G. *et al.* (2018) 'Surrogate data for hypothesis testing of physical systems', *Physics Reports*. Elsevier B.V., 748, pp. 1–60. doi: 10.1016/j.physrep.2018.06.001.

Laumann, T. O. *et al.* (2017) 'On the Stability of BOLD fMRI Correlations', *Cerebral Cortex*, 27(10), pp. 4719–4732. doi: 10.1093/cercor/bhw265.

Li, J., Kong, R., *et al.* (2019) 'Global signal regression strengthens association between resting-state functional connectivity and behavior', *NeuroImage*, 196, pp. 126–141. doi: 10.1016/j.neuroimage.2019.04.016.

Li, J., Bolt, T., *et al.* (2019) 'Topography and behavioral relevance of the global signal in the human brain.', *Scientific Reports*. Springer US, 10(September), pp. 1–5. doi: 10.1038/s41598-019-50750-8.

Liu, T. T., Nalci, A. and Falahpour, M. (2017) 'The global signal in fMRI: Nuisance or Information?', *NeuroImage*, 150(February), pp. 213–229. doi: 10.1016/j.neuroimage.2017.02.036.

Lurie, D. J. *et al.* (2019) 'Questions and controversies in the study of time-varying functional connectivity in resting fMRI', *Network Neuroscience*. doi: https://doi.org/10.1162/netn_a_00116.

Lydon-Staley, D. M. *et al.* (2019) 'Evaluation of confound regression strategies for the mitigation of micromovement artifact in studies of dynamic resting-state functional connectivity and multilayer network modularity', *Network Neuroscience*, 3(2), pp. 427–454. doi: 10.1162/netn.

Makowski, C., Lepage, M. and Evans, A. C. (2019) 'Head motion: The dirty little secret of neuroimaging in psychiatry',

Journal of Psychiatry and Neuroscience, 44(1), pp. 62–68. doi: 10.1503/jpn.180022.

Malik, M. *et al.* (2008) 'Subject-specific heart rate dependency of electrocardiographic QT, PQ, and QRS intervals', *Journal of Electrocardiology*. Elsevier Inc., 41(6), pp. 491–497. doi: 10.1016/j.jelectrocard.2008.06.022.

Mash, L. E. *et al.* (2019) 'Transient states of network connectivity are atypical in autism: A dynamic functional connectivity study', *Human Brain Mapping*, 40(8), pp. 2377–2389. doi: 10.1002/hbm.24529.

Matsui, T., Murakami, T. and Ohki, K. (2018) 'Neuronal Origin of the Temporal Dynamics of Spontaneous BOLD Activity Correlation', *Cerebral Cortex*, (August), pp. 1–13. doi: 10.1093/cercor/bhy045.

Mira-Dominguez, O. *et al.* (2014) 'Connectotyping: Model based fingerprinting of the functional connectome', *PLoS ONE*, 9(11). doi: 10.1371/journal.pone.0111048.

Van de Moortele, P. F. *et al.* (2002) 'Respiration-induced Bo fluctuations and their spatial distribution in the human brain at 7 Tesla', *Magnetic Resonance in Medicine*, 47(5), pp. 888–895. doi: 10.1002/mrm.10145.

Morgan, V. L. *et al.* (2017) 'Magnetic resonance imaging connectivity for the prediction of seizure outcome in temporal lobe epilepsy', *Epilepsia*, 58(7), pp. 1251–1260. doi: 10.1111/epi.13762.

Mueller, S. *et al.* (2013) 'Individual Variability in Functional Connectivity Architecture of the Human Brain', *Neuron*. Elsevier Inc., 77(3), pp. 586–595. doi: 10.1016/j.neuron.2012.12.028.

Murphy, K. and Fox, M. D. (2017) 'Towards a consensus regarding global signal regression for resting state functional connectivity MRI', *NeuroImage*. Elsevier, 154(November 2016), pp. 169–173. doi: 10.1016/j.neuroimage.2016.11.052.

Nalci, A., Luo, W. and Liu, T. T. (2019) 'Nuisance effects in inter-scan functional connectivity estimates before and after nuisance regression', *NeuroImage*, 202, p. 116005. doi: 10.1016/j.neuroimage.2019.07.018.

Nalci, A., Rao, B. D. and Liu, T. T. (2019) 'Nuisance effects and the limitations of nuisance regression in dynamic functional connectivity fMRI', *NeuroImage*. Elsevier Ltd, 184(September 2018), pp. 1005–1031. doi: 10.1016/j.neuroimage.2018.09.024.

Nikolaou, F. *et al.* (2016) 'Spontaneous physiological variability modulates dynamic functional connectivity in resting-state functional magnetic resonance imaging', *Philosophical Transactions of the Royal Society A: Mathematical, Physical and Engineering Sciences*, 374(2067), p. 20150183. doi: 10.1098/rsta.2015.0183.

Noble, S. *et al.* (2017) 'Influences on the Test-Retest Reliability of Functional Connectivity MRI and its Relationship with Behavioral Utility', *Cerebral Cortex*, 27(11), pp. 5415–5429. doi: 10.1093/cercor/bhx230.

Noll, D. C. and Schneider, W. (1994) 'Theory, simulation, and compensation of physiological motion artifacts in functional MRI', *Proceedings - International Conference on Image Processing, ICIP*, 3, pp. 40–44. doi: 10.1109/ICIP.1994.413892.

Ogawa, S. *et al.* (1990) 'Brain magnetic resonance imaging with contrast dependent on blood oxygenation', *Proc. Natl. Acad. Sci. USA*, 87, pp. 9868–9872. doi: 10.7566/JPSJ.84.064704.

Orban, C. *et al.* (2019) 'Time of day is associated with paradoxical reductions in global signal fluctuation and functional connectivity', *bioRxiv*.

Özbay, P. S. *et al.* (2019) 'Sympathetic activity contributes to the fMRI signal', *Communications Biology*. Springer US, 2(1), pp. 1–9. doi: 10.1038/s42003-019-0659-0.

Parkes, L. *et al.* (2018) 'An evaluation of the efficacy, reliability, and sensitivity of motion correction strategies for resting-state functional MRI', *NeuroImage*. Elsevier Ltd, 171(December 2017), pp. 415–436. doi: 10.1016/j.neuroimage.2017.12.073.

Pinna, G. D. *et al.* (2007) 'Heart rate variability measures: A fresh look at reliability', *Clinical Science*, 113(3–4), pp. 131–140. doi: 10.1042/CS20070055.

Pinto, J. *et al.* (2017) 'Improved 7 Tesla resting-state fMRI connectivity measurements by cluster-based modeling of respiratory volume and heart rate effects', *NeuroImage*. Elsevier, 153(April), pp. 262–272. doi: 10.1016/j.neuroimage.2017.04.009.

Pitzalis, M. V. *et al.* (1996) 'Short- and long-term reproducibility of time and frequency domain heart rate variability measurements in normal subjects', *Cardiovascular Research*, 32(2), pp. 226–233. doi: 10.1016/0008-6363(96)00086-7.

Power, J. D. *et al.* (2012) 'Spurious but systematic correlations in functional connectivity MRI networks arise from subject motion', *NeuroImage*. Elsevier Inc., 59(3), pp. 2142–2154. doi: 10.1016/j.neuroimage.2011.10.018.

Power, J. D. *et al.* (2014) 'Methods to detect, characterize, and remove motion artifact in resting state fMRI', *NeuroImage*. Elsevier Inc., 84, pp. 320–341. doi: 10.1016/j.neuroimage.2013.08.048.

Power, J. D. *et al.* (2017) 'Sources and implications of whole-brain fMRI signals in humans', *NeuroImage*. Elsevier, 146(September 2016), pp. 609–625. doi: 10.1016/j.neuroimage.2016.09.038.

Power, J. D. *et al.* (2018) 'Ridding fMRI data of motion-related influences: Removal of signals with distinct spatial and physical bases in multiecho data', *Proceedings of the National Academy of Sciences of the United States of America*, 115(9), pp. E2105–E2114. doi: 10.1073/pnas.1720985115.

Power, J. D. *et al.* (2019) 'Distinctions among real and apparent respiratory motions in human fMRI data', *NeuroImage*, 201. doi: 10.1101/601286.

Power, J. D. (2019) 'Temporal ICA has not properly separated global fMRI signals: A comment on Glasser et al. (2018)', *NeuroImage*. Elsevier Inc., (December 2018). doi: 10.1016/j.neuroimage.2018.12.051.

Power, J. D. *et al.* (2020) 'Characteristics of respiratory measures in young adults scanned at rest, including systematic changes and "missed" deep breaths', *NeuroImage*. Elsevier Inc., 204, p. 116234. doi: 10.1016/j.neuroimage.2019.116234.

Power, J. D., Schlaggar, B. L. and Petersen, S. E. (2015) 'Recent progress and outstanding issues in motion correction in resting state fMRI', *NeuroImage*. Elsevier Inc., 105, pp. 536–551. doi: 10.1016/j.neuroimage.2014.10.044.

Prokopiou, P. C. *et al.* (2019) 'Modeling of dynamic cerebrovascular reactivity to spontaneous and externally induced CO2 fluctuations in the human brain using BOLD-fMRI', *NeuroImage*. Elsevier Ltd, 186, pp. 533–548. doi: 10.1016/j.neuroimage.2018.10.084.

Pruim, R. H. R. *et al.* (2015) 'ICA-AROMA: A robust ICA-based strategy for removing motion artifacts from fMRI data', *NeuroImage*. Elsevier Inc., 112, pp. 267–277. doi: 10.1016/j.neuroimage.2015.02.064.

Quaegebeur, A., Lange, C. and Carmeliet, P. (2011) 'The neurovascular link in health and disease: Molecular mechanisms and therapeutic implications', *Neuron*. Elsevier Inc., 71(3), pp. 406–424. doi: 10.1016/j.neuron.2011.07.013.

Raichle, M. E. (2015) 'The Brain's Default Mode Network', *Annual Review of Neuroscience*, 38(1), pp. 433–447. doi: 10.1146/annurev-neuro-071013-014030.

Raj, D. *et al.* (2000) 'A model for susceptibility artefacts from respiration in functional echo-planar magnetic resonance imaging', *Physics in Medicine and Biology*, 45(12), pp. 3809–3820. doi: 10.1088/0031-9155/45/12/321.

Raj, D., Anderson, A. W. and Gore, J. C. (2001) 'Respiratory effects in human functional magnetic resonance imaging due to bulk susceptibility changes', *Physics in Medicine and Biology*, 46(12), pp. 3331–3340. doi: 10.1088/0031-9155/46/12/318.

Reland, S. *et al.* (2005) 'Reliability of heart rate variability in healthy older women at rest and during orthostatic testing', *Aging Clinical and Experimental Research*, 17(4), pp. 316–321. doi: 10.1007/BF03324616.

Robinson, E. C. *et al.* (2014) 'MSM: A new flexible framework for multimodal surface matching', *NeuroImage*, 100, pp. 414–426. doi: 10.1016/j.neuroimage.2014.05.069.

Sakoglu, U. *et al.* (2010) 'A method for evaluating dynamic functional network connectivity and task-modulation: Application to schizophrenia', *Magnetic Resonance Materials in Physics, Biology and Medicine*. doi: 10.1007/s10334-010-0197-8.

Sala-Llonch, R., Bartrés-Faz, D. and Junqué, C. (2015) 'Reorganization of brain networks in aging: a review of functional connectivity studies.', *Frontiers in psychology*, 6(May), p. 663. doi: 10.3389/fpsyg.2015.00663.

Salimi-Khorshidi, G. *et al.* (2014) 'Automatic denoising of functional MRI data: Combining independent component analysis and hierarchical fusion of classifiers', *NeuroImage*. Elsevier B.V., 90, pp. 449–468. doi: 10.1016/j.neuroimage.2013.11.046.

Satterthwaite, T. D. *et al.* (2012) 'Impact of in-scanner head motion on multiple measures of functional connectivity: Relevance for studies of neurodevelopment in youth', *NeuroImage*. Elsevier Inc., 60(1), pp. 623–632. doi: 10.1016/j.neuroimage.2011.12.063.

Satterthwaite, T. D. *et al.* (2013) 'An improved framework for confound regression and filtering for control of motion artifact in the preprocessing of resting-state functional connectivity data', *NeuroImage*. Elsevier Inc., 64(1), pp. 240–256. doi: 10.1016/j.neuroimage.2012.08.052.

Schölvinck, M. L. *et al.* (2010) 'Neural basis of global resting-state fMRI activity.', *Proceedings of the National Academy of Sciences of the United States of America*, 107(22), pp. 10238–43. doi: 10.1073/pnas.0913110107.

Seitzman, B. A., Gratton, C., Marek, S., *et al.* (2019) 'A set of functionally-defined brain regions with improved representation of the subcortex and cerebellum', *NeuroImage*, p. 116290. doi: 10.1016/j.neuroimage.2019.116290.

Seitzman, B. A., Gratton, C., Laumann, T. O., *et al.* (2019) 'Trait-like variants in human functional brain networks', *Proceedings of the National Academy of Sciences*. doi: 10.1073/pnas.1902932116.

Shannon, B. J. *et al.* (2013) 'Morning-evening variation in human brain metabolism and memory circuits', *Journal of Neurophysiology*, 109(5), pp. 1444–1456. doi: 10.1152/jn.00651.2012.

Shmuel, A. and Leopold, D. A. (2008) 'Neuronal correlates of spontaneous fluctuations in fMRI signals in monkey visual cortex: Implications for functional connectivity at rest', *Human Brain Mapping*, 29(7), pp. 751–761. doi: 10.1002/hbm.20580.

Shmueli, K. *et al.* (2007) 'Low-frequency fluctuations in the cardiac rate as a source of variance in the resting-state fMRI BOLD signal', *NeuroImage*, 38(2), pp. 306–320. doi: 10.1016/j.neuroimage.2007.07.037.

Smith, S. M. *et al.* (2009) 'Correspondence of the brain's functional architecture during activation and rest.', *Proceedings of the National Academy of Sciences of the United States of America*, 106(31), pp. 13040–5. doi: 10.1073/pnas.0905267106.

Smith, S. M. *et al.* (2013) 'Resting-state fMRI in the Human Connectome Project', *NeuroImage*, 80, pp. 144–168. doi: 10.1016/j.neuroimage.2013.05.039.

Tagliazucchi, E. and Laufs, H. (2014) 'Decoding Wakefulness Levels from Typical fMRI Resting-State Data Reveals Reliable Drifts between Wakefulness and Sleep', *Neuron*. Elsevier Inc., 82(3), pp. 695–708. doi: 10.1016/j.neuron.2014.03.020.

Thompson, G. J., Merritt, M. D., *et al.* (2013) 'Neural correlates of time-varying functional connectivity in the rat', *NeuroImage*. Elsevier Inc., 83, pp. 826–836. doi: 10.1016/j.neuroimage.2013.07.036.

Thompson, G. J., Magnuson, M. E., *et al.* (2013) 'Short-time windows of correlation between large-scale functional brain networks predict vigilance intraindividually and interindividually', *Human Brain Mapping*, 34(12), pp. 3280–3298. doi: 10.1002/hbm.22140.

Tong, Y. *et al.* (2013) 'Evaluating the effects of systemic low frequency oscillations measured in the periphery on the independent component analysis results of resting state networks', *NeuroImage*. Elsevier Inc., 76, pp. 202–215. doi: 10.1016/j.neuroimage.2013.03.019.

Tong, Y. and Frederick, B. de B. (2014) 'Studying the spatial distribution of physiological effects on BOLD signals using ultrafast fMRI', *Frontiers in Human Neuroscience*, 8(1 APR), pp. 1–8. doi: 10.3389/fnhum.2014.00196.

Tong, Y., Hocke, L. M. and Frederick, B. B. (2019) 'Low Frequency Systemic Hemodynamic "Noise" in Resting State BOLD fMRI: Characteristics, Causes, Implications, Mitigation Strategies, and Applications', *Frontiers in Neuroscience*, 13(August). doi: 10.3389/fnins.2019.00787.

Valenza, G. *et al.* (2019) 'The central autonomic network at rest: Uncovering functional MRI correlates of time-varying autonomic outflow', *NeuroImage*. Elsevier Inc. doi: 10.1016/j.neuroimage.2019.04.075.

Vanderwal, T. *et al.* (2017) 'Individual differences in functional connectivity during naturalistic viewing conditions', *NeuroImage*, 157(June), pp. 521–530. doi: 10.1016/j.neuroimage.2017.06.027.

Vidaurre, D. *et al.* (2018) 'Spontaneous cortical activity transiently organises into frequency specific phase-coupling networks', *Nature Communications*. Springer US, 9(2987). doi: 10.1038/s41467-018-05316-z.

Vigneau-Roy, N. *et al.* (2014) 'Regional variations in vascular density correlate with resting-state and task-evoked blood oxygen level-dependent signal amplitude', *Human Brain Mapping*, 35(5), pp. 1906–1920. doi: 10.1002/hbm.22301.

Wang, C. *et al.* (2016) 'Spontaneous eyelid closures link vigilance fluctuation with fMRI dynamic connectivity states', *Proceedings of the National Academy of Sciences*, 113(34), pp. 9653–9658. doi: 10.1073/pnas.1523980113.

Whittaker, J. R. *et al.* (2019) 'Cerebral autoregulation evidenced by synchronized low frequency oscillations in blood pressure and resting-state fMRI', *Frontiers in Neuroscience*, 13(MAY), pp. 1–12. doi: 10.3389/fnins.2019.00433.

Winder, A. T. *et al.* (2017) 'Weak correlations between hemodynamic signals and ongoing neural activity during the resting state', *Nature Neuroscience*. Springer US, 20(12), pp. 1761–1769. doi: 10.1038/s41593-017-0007-y.

Wise, R. G. *et al.* (2004) 'Resting fluctuations in arterial carbon dioxide induce significant low frequency variations in BOLD signal', *NeuroImage*, 21(4), pp. 1652–1664. doi: 10.1016/j.neuroimage.2003.11.025.

Wong, C. K. *et al.* (2016) 'Automatic EEG-assisted retrospective motion correction for fMRI (aE-REMCOR)', *NeuroImage*. The Authors, 129, pp. 133–147. doi: 10.1016/j.neuroimage.2016.01.042.

Wong, C. W. *et al.* (2013) 'The amplitude of the resting-state fMRI global signal is related to EEG vigilance measures', *NeuroImage*. Elsevier Inc., 83, pp. 983–990. doi: 10.1016/j.neuroimage.2013.07.057.

Xia, C. H. *et al.* (2018) 'Linked dimensions of psychopathology and connectivity in functional brain networks', *Nature Communications*. Springer US, 9(1), pp. 1–14. doi: 10.1038/s41467-018-05317-y.

Xia, Y. *et al.* (2019) 'Tracking the dynamic functional connectivity structure of the human brain across the adult lifespan', *Human Brain Mapping*, 40(3), pp. 717–728. doi: 10.1002/hbm.24385.

Yan, C. G. *et al.* (2013) 'A comprehensive assessment of regional variation in the impact of head micromovements on functional connectomics', *NeuroImage*. Elsevier Inc., 76, pp. 183–201. doi: 10.1016/j.neuroimage.2013.03.004.

Zeng, L.-L. *et al.* (2014) 'Neurobiological basis of head motion in brain imaging', *Proceedings of the National Academy of Sciences*, 111(16), pp. 6058–6062. doi: 10.1073/pnas.1317424111.

Zhang, J. *et al.* (2019) 'Intrinsic Architecture of Global Signal Topography and Its Modulation by Tasks', *bioRxiv*.

Zilles, K. *et al.* (1988) 'The human pattern of gyrification in the cerebral cortex', *Anatomy and Embryology*, 179(2), pp. 173–179. doi: 10.1007/BF00304699.

Supplementary material

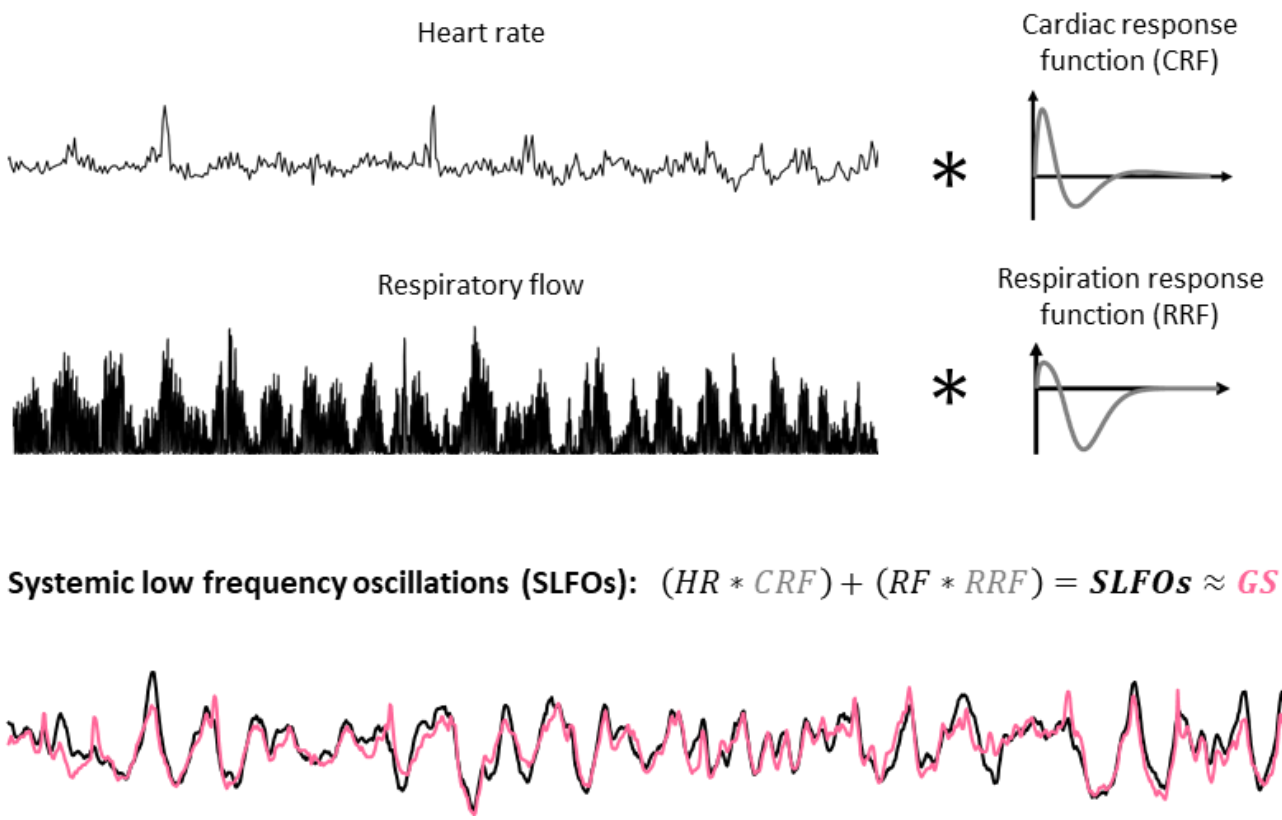

Supp. Fig. 1. Illustration of how the traces of heart rate and breathing activity were used to model the systemic low frequency oscillations (SLFOs). The respiratory flow was defined as the square of the derivative of the breathing signal. The cardiac and respiration response functions were estimated separately for each scan, using the methodology proposed in (Kassinopoulos and Mitsis, 2019a). Heart rate and respiratory flow were convolved with the cardiac and respiration response functions, respectively, in order to obtain the fluctuations of SLFOs. As can be seen in the example, SLFOs have high correlation with the global signal (GS; the average correlation is 0.65 across all scans considered in this study).

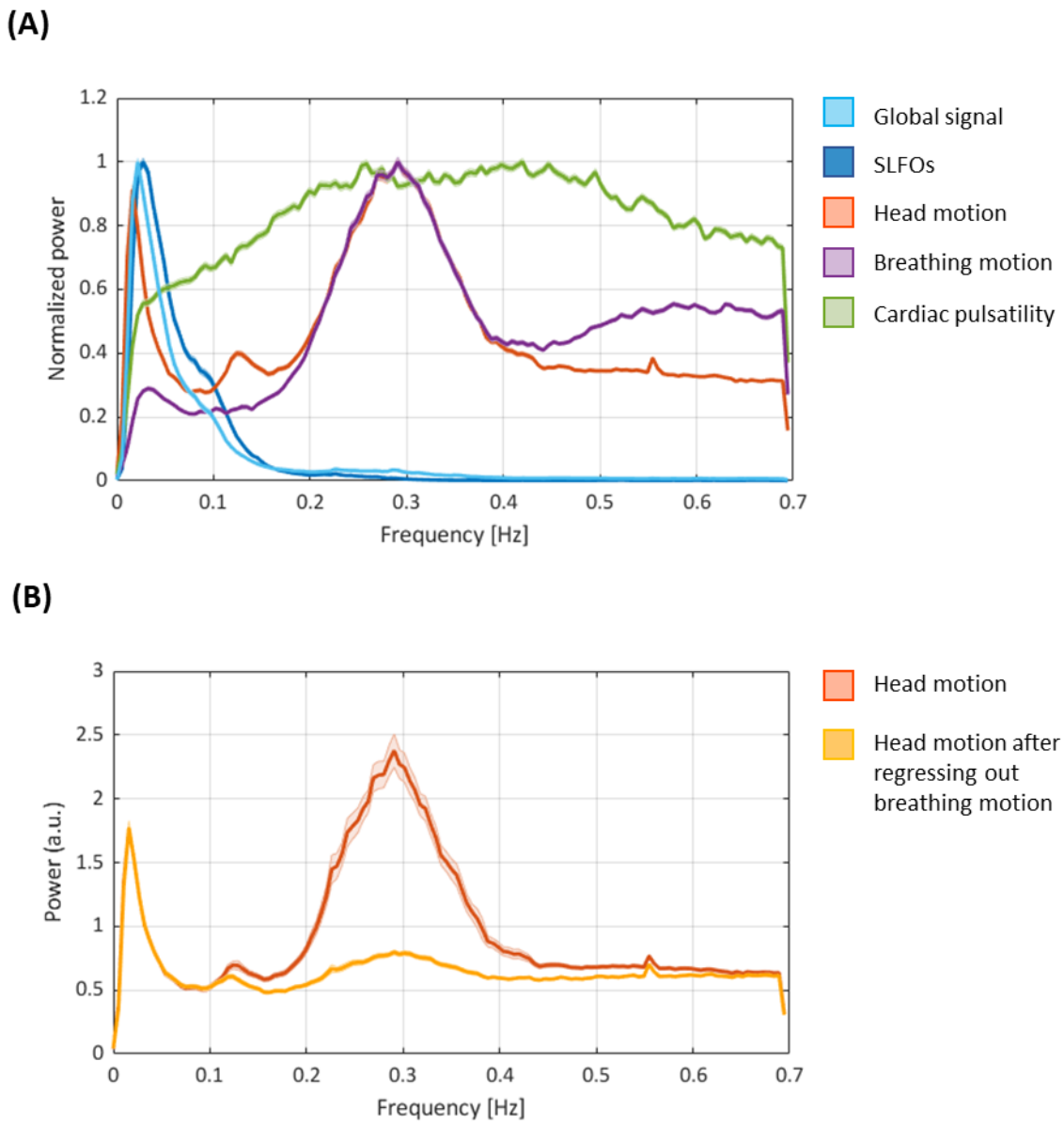

Supp. Fig. 2. (A) Power spectral densities of the nuisance processes evaluated in this study (as well as the global signal for reference). SLFOs mostly carry low-frequency fluctuations (<0.15 Hz). Breathing motion exhibits a peak at ~0.3 Hz, consistent with the average breathing rate across subjects. Head motion exhibits the same 0.3 Hz peak, underscoring the observation that realignment parameters are contaminated by breathing. We also observe a peak in head motion at ~0.12 Hz, recently attributed to deep breaths (Power et al. 2019), and a very narrow peak at 0.55 Hz that is likely due to scanner artifacts. The fMRI data is not sampled fast enough to capture cardiac pulsatility (~1 Hz), hence cardiac activity is aliased into a range of frequencies. Thus, any variation in heart rate during a scan as well as across subjects is likely to spread cardiac pulsatility artifacts into different frequencies, broadening the spectral peak. **(B)** Power spectral density of head motion before and after regressing out breathing motion. Note the substantial decrease in power around 0.3 Hz after removing the effect of breathing motion.

Both figures show the mean and standard error across subjects for scan Rest1_LR (similar results were observed for all other scans).

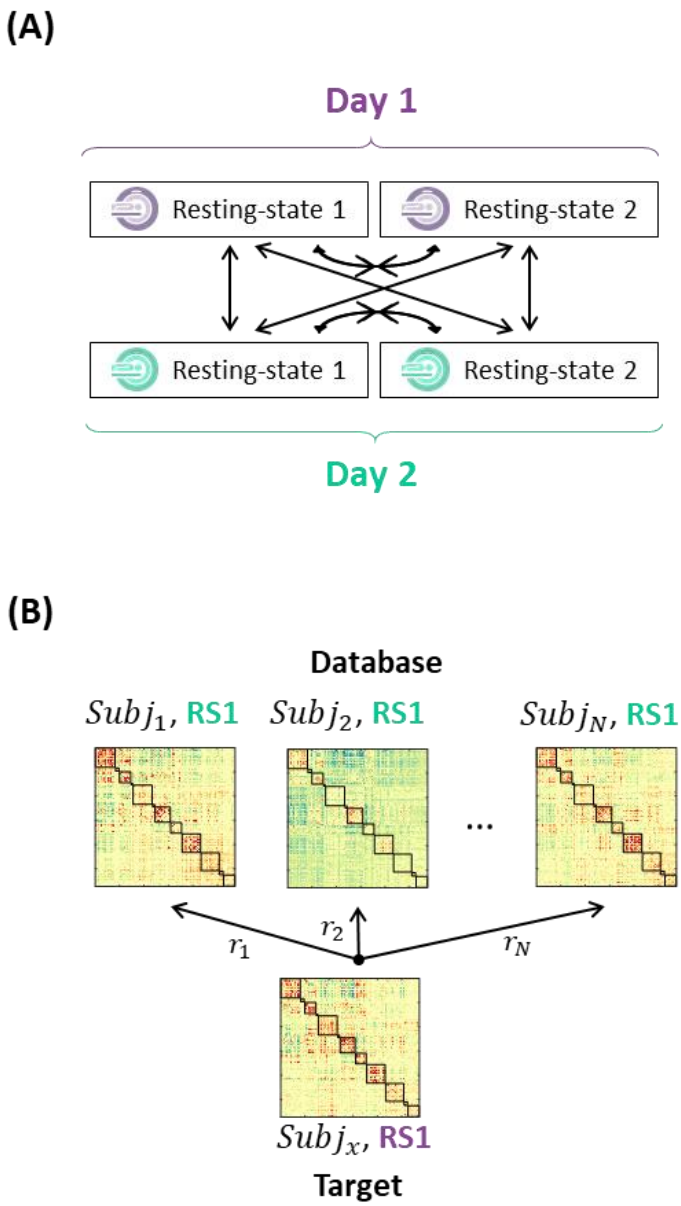

$$ID_{Subj_x} = \begin{cases} 1 & argmax(r_1, r_2, \ldots, r_N) = x \\ 0 & argmax(r_1, r_2, \ldots, r_N) \neq x \end{cases}$$

$$Accuracy_{RS1 \rightarrow RS1} = \frac{1}{N} \sum_{n=1}^{N} ID_{Subj_n}$$

Supp. Fig. 3. Connectome fingerprinting. (A) Diagram of the target-database combinations between resting-state scans. **(B)** Example on how to compute the identification accuracy for a target-database pair. Figure based on Finn et al. (2015).

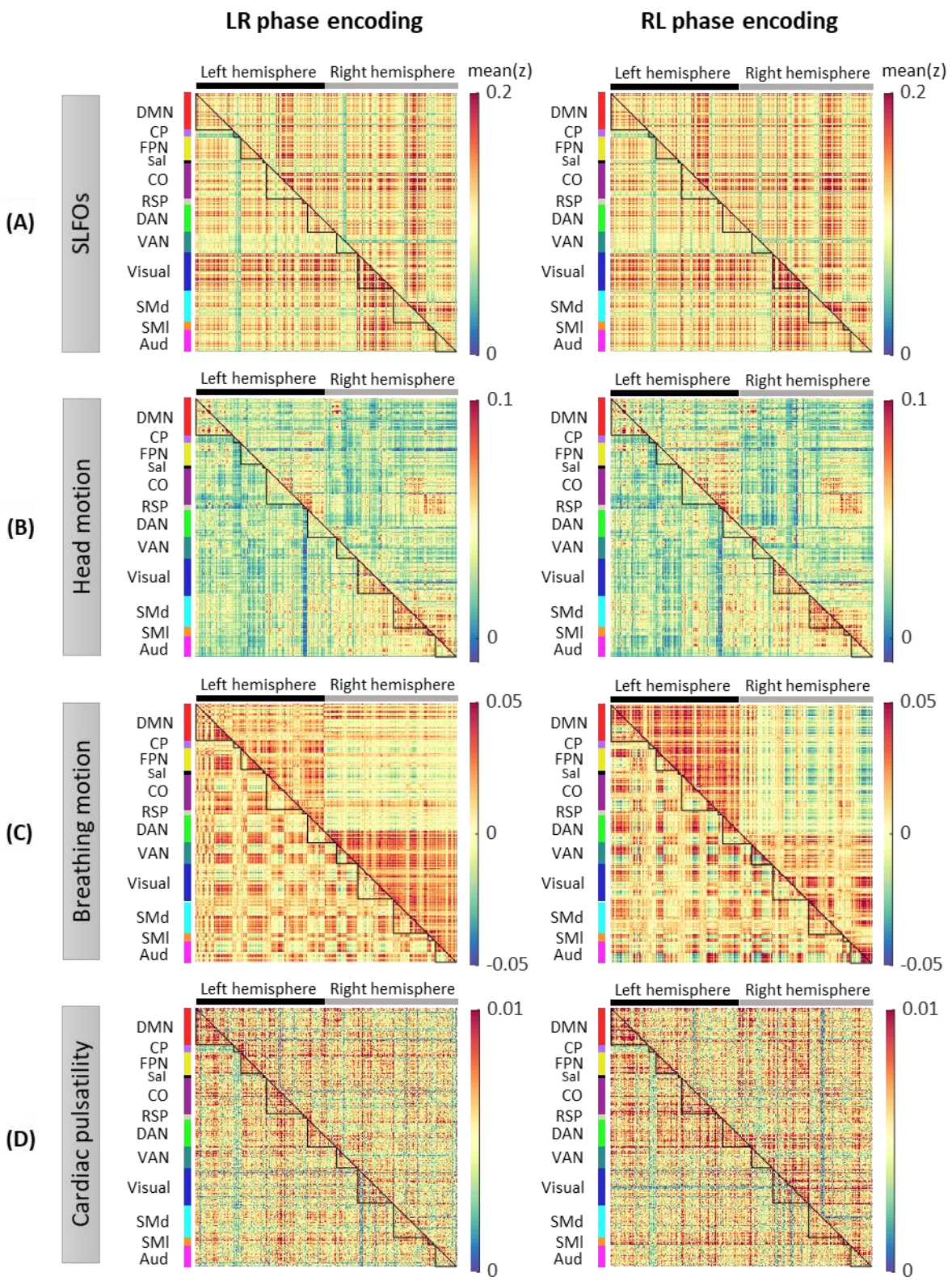

Supp. Fig. 4. Static FC. Group averaged nuisance FC matrices across 784 scans based on their LR and RL phase encoding direction for **(A)** SLFOs, **(B)** head motion, **(C)** breathing motion, and **(D)** cardiac pulsatility.

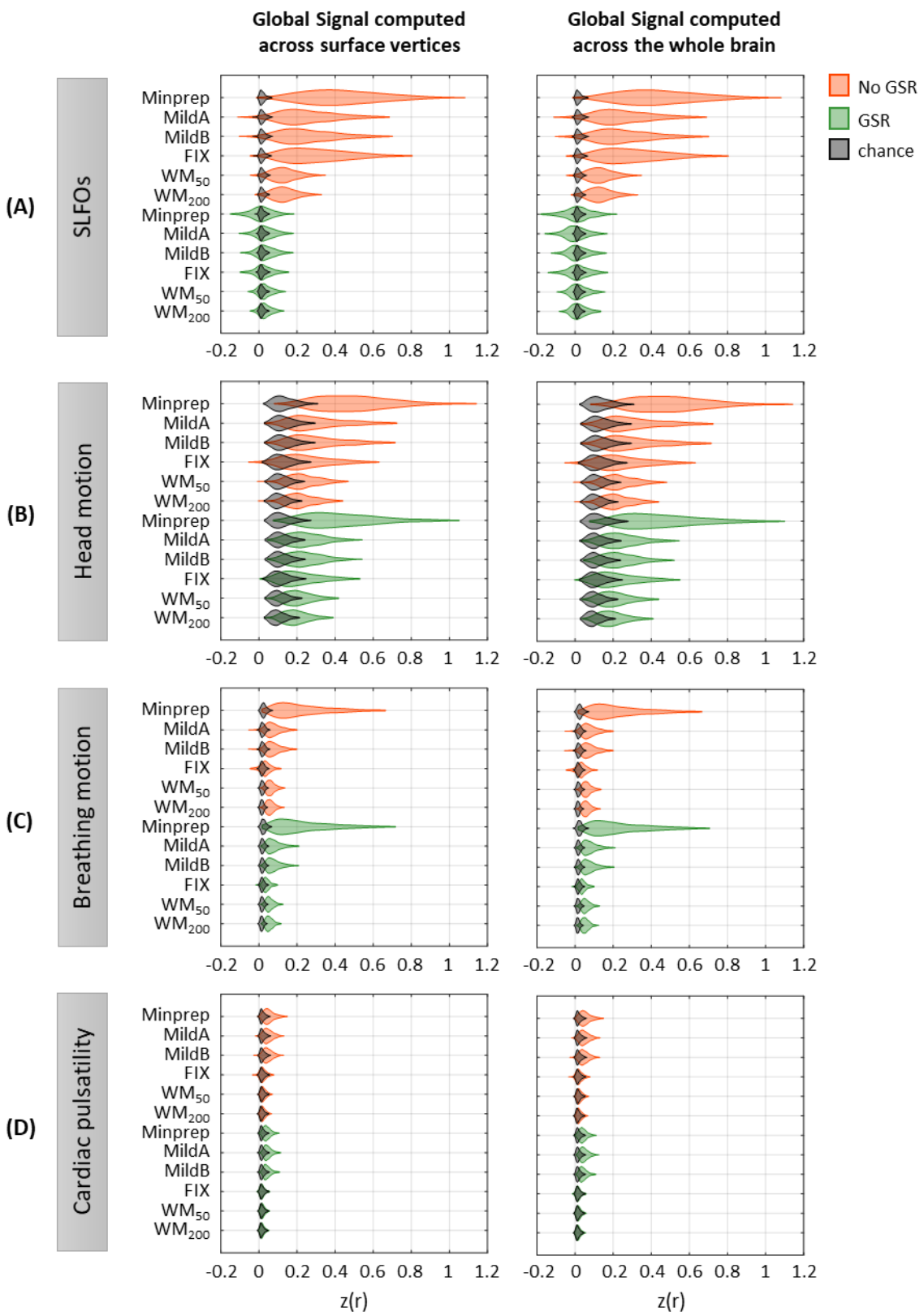

Supp. Fig. 5. Static FC. Distribution of Pearson correlation coefficients across all 1,568 scans between the "neural" FC matrix after each preprocessing pipeline and nuisance FC matrices associated to **(A)** SLFOs, **(B)** head motion, **(C)** breathing motion, and **(D)** cardiac pulsatility, both when the global signal was computed across vertices in surface space (left column), and when the global signal was computed across the whole brain in volumetric space (right column). Correlation values were Fisher z transformed. Note that correlation coefficients identified as outliers (> 3 SD) were disregarded.

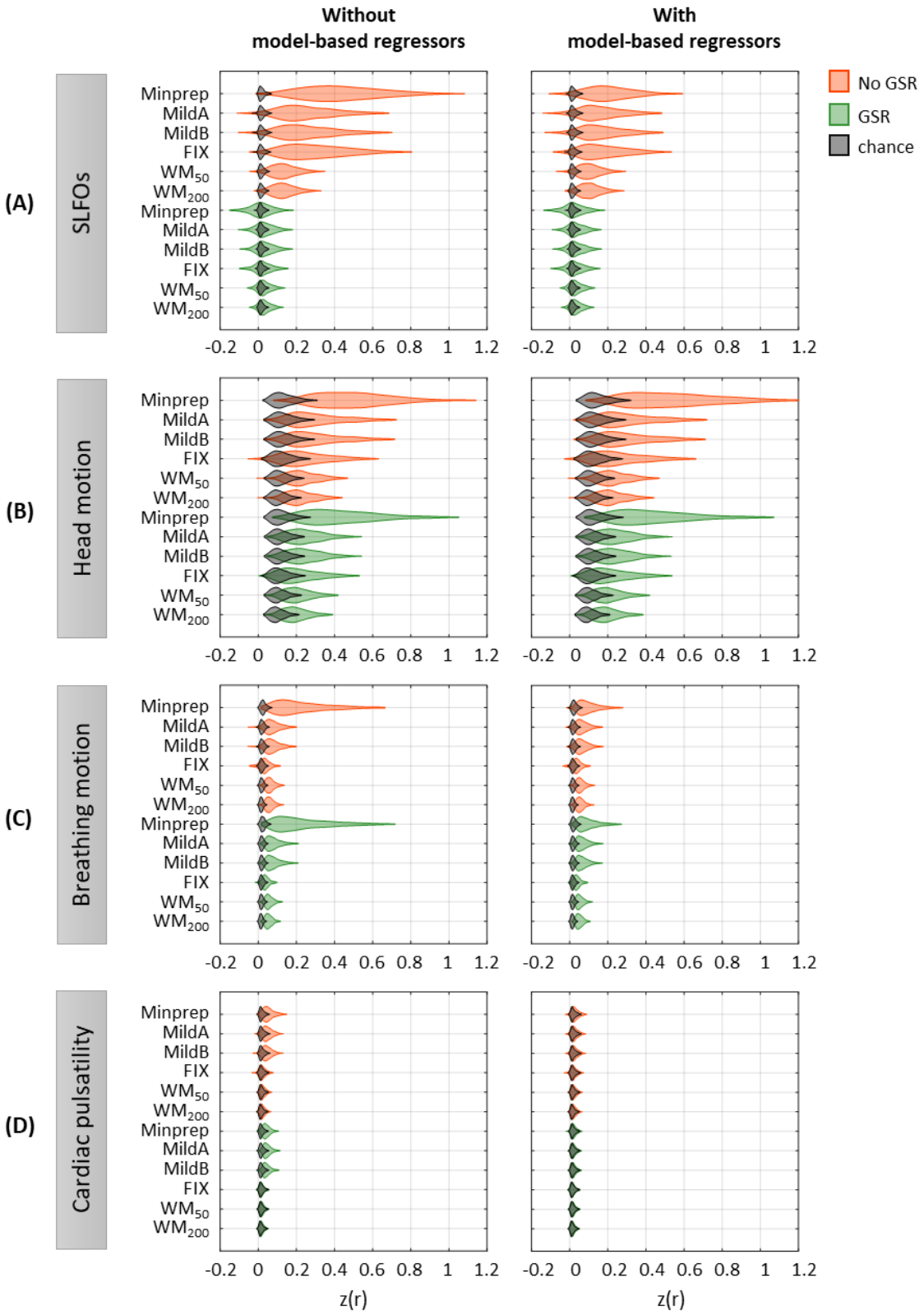

Supp. Fig. 6. Static FC. Distribution of Pearson correlation coefficients across all 1,568 runs between the "neural" FC matrix after each preprocessing pipeline and nuisance FC matrices associated to **(A)** SLFOs, **(B)** head motion, **(C)** breathing motion, and **(D)** cardiac pulsatility, when physiological regressors obtained from model-based techniques were included (right column) or not (left column) as nuisance regressors in the preprocessing strategies. Correlation values were Fisher z transformed. Note that correlation coefficients identified as outliers (> 3 SD) were disregarded.

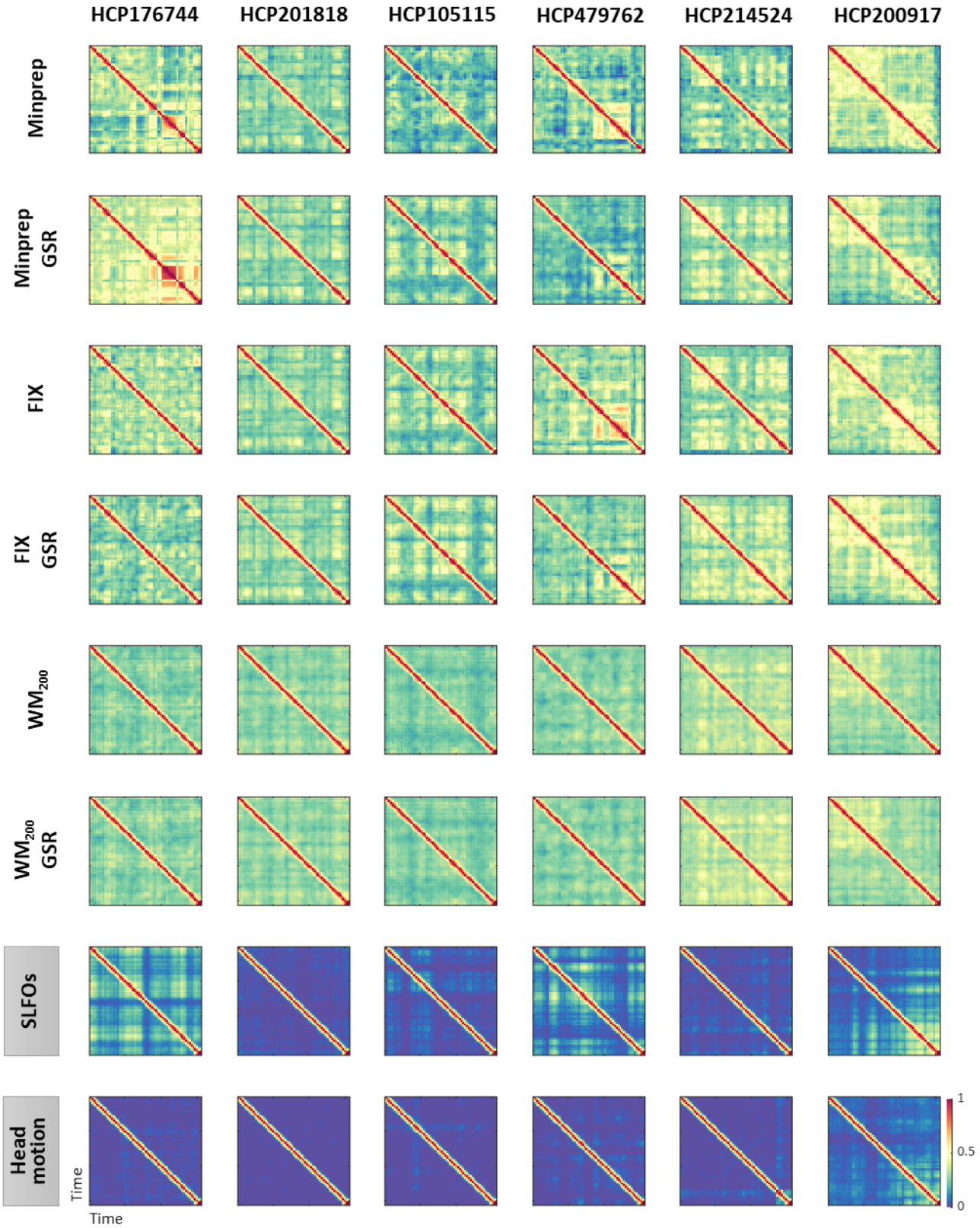

Supp. Fig. 7. Time-varying FC. Illustrative examples of FCD matrices from specific HCP subjects for several preprocessing pipelines (rows 1-6) and SLFOs and head motion (rows 7 and 8, respectively). All the examples are from the HCP scan Rest1_LR. These subjects did not show a large resemblance between FCD matrices computed from the "neural" datasets and FCD matrices computed from the nuisance datasets of SLFOs and head motion. Note that the WM200 preprocessing strategy substantially diminished the recurrent FC patterns.

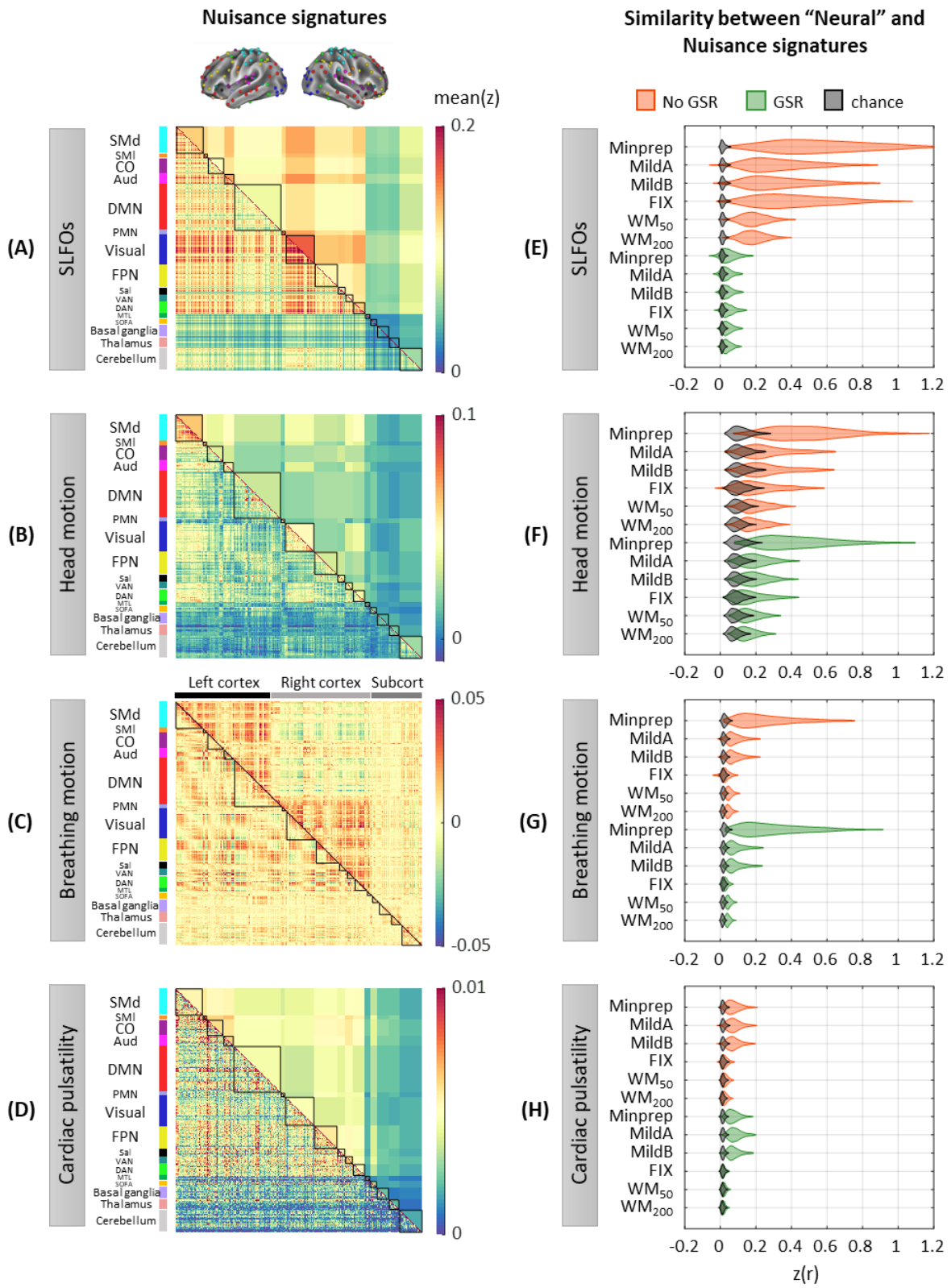

Supp. Fig. 8. Static FC results for the Seitzman atlas. (A-D) Group averaged "physiological" FC across all 1,568 scans for **(A)** SLFOs, **(B)** head motion, **(C)** breathing motion, and **(D)** cardiac pulsatility. **(E-H)** Distribution of Pearson correlation coefficients across all 1,568 scans between the "neural" FC matrix after each preprocessing pipeline and nuisance FC matrices associated to **(E)** SLFOs, **(F)** head motion, **(G)** breathing motion, and **(H)** cardiac pulsatility. Correlation values were Fisher z transformed. Note that correlation coefficients identified as outliers (> 3 SD) were disregarded.

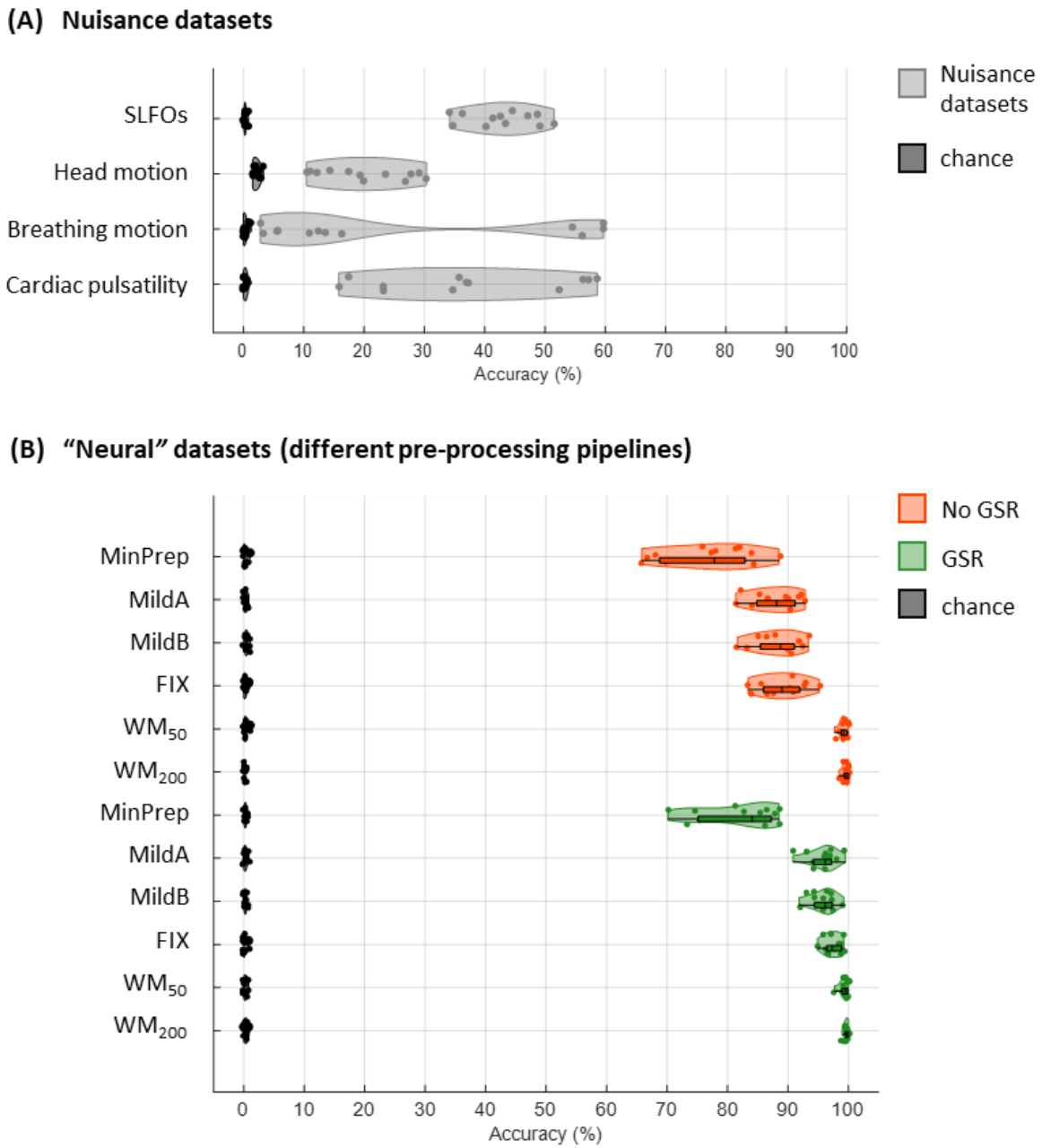

Supp. Fig. 9. Connectome fingerprinting results for the Seitzman atlas. (A) Fingerprinting accuracy obtained using the static FC matrices from the generated nuisance datasets where non-neural fluctuations were isolated from the BOLD data. **(B)** Fingerprinting accuracy obtained using the static FC matrices generated from each of the preprocessing strategies evaluated.

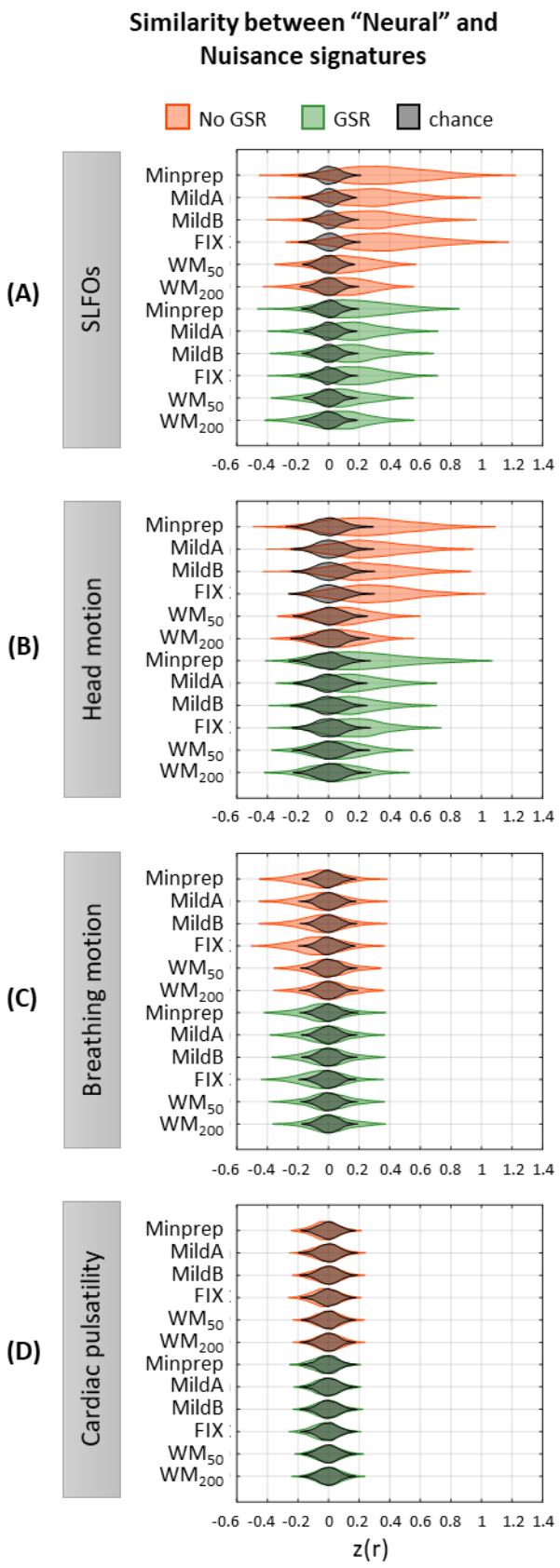

Supp. Fig. 10. Time-varying FC results for the Seitzman atlas.

Distribution of Pearson correlation coefficients across all 1,568 scans between the "neural" FCD matrix after each preprocessing pipeline and nuisance FCD matrices associated to **(A)** SLFOs, **(B)** head motion, **(C)** breathing motion, and **(D)** cardiac pulsatility. Correlation values were Fisher z transformed. Note that correlation coefficients identified as outliers (> 3 SD) were disregarded.